Journal Pre-proof

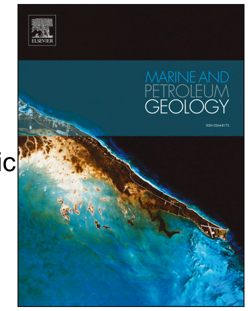

Shallow subsurface fluid dynamics in the Malvinas Basin (SW Atlantic): A geoacoustic analysis

J.P. Ormazabal, E. Lodolo, M.E. Bravo, S. Principi, F.I. Palma, D.M. Bran, J.I. Isola, F.D. Esteban, A.A. Tassone

PII: S0264-8172(24)00461-6

DOI: https://doi.org/10.1016/j.marpetgeo.2024.107149

Reference: JMPG 107149

To appear in: *Marine and Petroleum Geology*

Received Date: 3 February 2024

Revised Date: 2 October 2024

Accepted Date: 4 October 2024

Please cite this article as: Ormazabal, J.P., Lodolo, E., Bravo, M.E., Principi, S., Palma, F.I., Bran, D.M., Isola, J.I., Esteban, F.D., Tassone, A.A., Shallow subsurface fluid dynamics in the Malvinas Basin (SW Atlantic): A geoacoustic analysis, *Marine and Petroleum Geology*, https://doi.org/10.1016/j.marpetgeo.2024.107149.

Shallow subsurface fluid dynamics in the Malvinas Basin (SW Atlantic): A geoacoustic analysis

J. P. Ormazabal[1,2], *E. Lodolo*[3], *M.E. Bravo*[1,2], *S. Principi*[1,2,4], *F.I. Palma*[1,2], *D.M. Bran*[1,2], *J.I. Isola*[1,2,5], *F.D. Esteban*[1,2], *A.A. Tassone*[1,2]

[1]*Universidad de Buenos Aires, Facultad de Ciencias Exactas y Naturales, Depto. De Ciencias Geológicas, Ciudad Universitaria Pabellón 2, Buenos Aires, Argentina*

[2]*CONICET-Universidad de Buenos Aires, Instituto de Geociencias Básicas, Aplicadas y Ambientales de Buenos Aires (IGeBA), Buenos Aires, Argentina*

[3]*Istituto Nazionale di Oceanografia e di Geofisica Sperimentale (OGS), Trieste, Italy*

[4]*YPF Tecnología S.A (Y-TEC), Provincia de Buenos Aires, Argentina*

[5]*Department of Geological Sciences, Rutgers, The State University of New Jersey, USA.*

Highlights

- Genesis of seep sites varies within the same anticlinal structure.
- Seabed extensional faults drive the formation of pockmarks and a carbonate mound.
- Anticlines are the most important regulators in the fluid plumbing system.
- Staggered BSRs allowed fluids to seep into the seafloor.

Abstract

Using a database consisting of sub-bottom profiles, 2D and 3D seismic data, a series of seep structures and acoustic anomalies associated with a plumbing system in the subsurface of the southern part of the Malvinas Basin off the Argentine coast are presented. The seep morphologies consist of mounds, pockmarks, and a carbonate mound, derived from hydrocarbons migrating from the Early Cretaceous Springhill and Lower Inoceramus formations through extensional faults and overthrusts of the Malvinas Fold-Thrust Belt and accumulating in the gas hydrate stability zone. This configuration is widely observed in the anticlines of the Malvinas Fold-Thrust Belt, which are characterized by a vertical structure highlighting a Bottom Simulating Reflector (BSR) overlain by a blanked-out zone at the seabed, interpreted as a gas hydrate stability zone. The plumbing system is influenced by active transtensional tectonics, as shown by two sets of extensional faults concentrated over some anticlines. These faults lead to displacements that, in many cases, reach the seabed. One nuance of the influence of tectonic activity on fluid escape is most evident in the Malvinas anticline, where all the pockmarks and the carbonate mound are concentrated. In the western part of the Malvinas anticline, five

pockmarks are observed in an area characterized by a shallow BSR. In contrast, in the eastern part of the Malvinas Basin, one pockmark and one carbonate mound are derived from a series of extensional faults. The presented data, as well as a comparison between the western and eastern parts of the Malvinas anticline, indicate that the anticlines are the main cause of seepage in this area, as they allow the accumulation of migrating fluids. Likewise, the seepage morphologies outside the anticlines are much less pronounced, as can be observed in the mounds that overlie the bottom vents.

Keywords: Malvinas Basin, Fluid seepage, Pockmark, Carbonate Mound, Fold-thrust belt

1. Introduction

Plumbing systems and seepage morphologies form through the migration of fluids and their discharge into the water column. The intensity and volume of fluid flow, as well as the interaction of fluids with the water-seabed interface and sub-surface piping systems are among the most important controlling factors for the geomorphologic expression of hydrocarbon seepage at the seabed (Böttner et al., 2019; Cole et al., 2000; Gay et al., 2006; Judd and Hovland, 2007; Kunath et al., 2022; Ma et al., 2021; Talukder, 2012). Pockmarks are one of the simplest seep morphologies, consisting of a depression formed by the collapse of the sediment upon upward migration of overpressured fluids (brine, freshwater, and methane gas), which lead to the erosion of surface sediments that are later redistributed by currents (Böttner et al., 2019; Ceramicola et al., 2018; Gay et al., 2007; Hovland and Judd., 1988; Wildish et al., 2008).

Besides pockmarks, the seeping of fluids from depth can produce elevated bathymetric features (Kopf, 2002; Paull et al., 2008). These structures are descriptively referred to as mounds, including landforms under specific conditions such as mud volcanoes or pingoes (Hovland and Svensen, 2006; Kim et al., 2020; Serié et al., 2012). For mud volcanoes, their genesis involves a higher pressure and deeper source than that required for the pockmark formation (Dimitrov, 2002; Kopf, 2002; Savini et al., 2009; Soto and Hudec, 2023), which can result from compressional tectonics (Ceramicola et al., 2018). Methane is almost always the predominant gas, and the derived carbonate structures produce consistent erupted material that contributes to the conical shape of these structures (Dimitrov, 2002; Kvenvolden and Barnard, 1983; Milkov, 2000; Pape et al., 2014; Reed et al., 1990; Tinivella and Giustiniani, 2012). The subsurface structure associated with mud volcanoes includes a bicone-shaped volcanic edifice underlain by a downward-tapering cone of collapsed country rock (Davies and Stewart, 2005). Other types of mounds include carbonate mounds and hydrate mounds (*i.e.* pingoes), among various positive structures that can be associated with gas activity, particularly in areas with gas hydrate formation (Chen et al., 2020; Hovland and Svensen, 2006; Serié et al., 2012). Other types of seabed structures associated with gas seepage include Methane-Derived Autigenic Carbonates (MDACs), which are authigenic carbonate minerals precipitated in situ within marine sediments or seafloor (Akam et al., 2023; Magalhães et al., 2012). With higher methane flux rates, MDACs can accumulate at the sediment-seawater interface as pavements or crusts of carbonates, while with lower flux the accumulation can occur below the seafloor through cementation along pipes (Ceramicola et al., 2018).

Due to the genetic connotation of mud volcanoes, carbonate mounds, hydrate mounds, and pockmarks, their classification should be approached with caution. These features are widespread globally, but in many areas, they have only recently been discovered (e.g., Idczak et al., 2020; Mordukhovich et al., 2023). The continental margins of the southwestern Atlantic Ocean have the potential to host hydrocarbon seeps but still remain an underexplored area of the global ocean (Kennedy and Rotjan, 2023). In the Argentine continental margin, despite the recognized hydrocarbon reservoirs, reported pockmarks and mounds are so far sparse and unclear (Anka et al*.,* 2014; Gómez et al., 2016; DeVito and Kearns, 2022). However, recent studies have identified a large area of the continental slope of the Argentine Exclusive Economic Zone covered by kilometer-sized pockmarks (Isola et al., 2021, 2020). On the other hand, a mud volcano-like structure and mounds have also been described in the same region (Isola et al., 2020; Muñoz et al., 2012). Further exploration is required to map the extent of surface manifestations of possible hydrocarbon reservoirs.

The Malvinas Basin is an offshore basin in the southernmost part of South America, where a proven petroleum system has been documented (Fig. 1A; Galeazzi, 1998; Raggio et al., 2011; DeVito and Kearns, 2022). The units in the southern part of the Malvinas Basin were incorporated into the Malvinas Fold-Thrust Belt (MFTB, Tassone et al., 2008; Ghiglione et al., 2010; Ormazabal et al., 2019). Baristeas et al. (2012) indicated the existence of an active gas plumbing system with a thermogenic source in the MFTB. Appropriate physical conditions and acoustic evidence led different authors to demonstrate the existence of a Bottom Simulating Reflector (BSR) and a Gas Hydrate Stability Zone (GHSZ) with a thermogenic origin in the southern part of the basin (Baristeas et al., 2012; Gómez et al., 2016). A similar configuration of the gas plumbing system and fold-thrust belt observed in the Malvinas Basin can be found in the adjacent South Malvinas/Falkland Basin to the east (Bry et al., 2004; Foschi et al., 2019; Foschi and Cartwright, 2016).

In this work, we use 2D and 3D seismic data, along with recently acquired sub-bottom profiles, to identify and map a series of pockmarks and a carbonate mound that have not been previously documented in the literature. The plumbing system is analyzed in the context of the Malvinas hydrocarbon system, considering the role of the MFTB and extensional faults formed by transtensional tectonics.

2. Geodynamic Background

2.1 Geodynamic setting

This study is conducted in the southern part of the Malvinas Basin, which lies north of the North Scotia Ridge (NSR, Fig. 1A). The Malvinas Basin is a Cenozoic foreland basin overlying a Mesozoic back-arc basin (Yrigoyen, 1989; Galeazzi, 1998; Tassone et al., 2008). In the southern part of the Malvinas Basin, the deposits were deformed and integrated into the MFTB due to the convergence of the Burdwood Bank and the Fuegian backstop against the Tierra del Fuego and Malvinas shelves (Esteban, 2014; Torres Carbonell et al., 2014). The position of the MFTB is consistent with underlying structures, particularly extensional faults within Mesozoic sequences that primarily affect units below the MFTB, some of which show tectonic inversion (Ormazabal et al., 2020, 2019). Ormazabal et al. (2024) described the MFTB in the study area as a buried configuration that flattens out to the south until it reaches the seabed (Fig. 2A and Fig. 3A). The anticlines of the MFTB present an ENE-WSW to ESE-WNW orientation and have been described as NNW-verging thrust hanging wall anticlines. This vergence is less conspicuous in the Malvinas anticline, a complex E-W oriented structure with symmetrical limbs interpreted as a combination of a thrust-related fold and a detachment fold, converging with the inner ENE-WSW oriented anticlines east of 62°30’ W (Fig. 2C; Ormazabal et al. 2024).

The NSR is a morphostructural system that marks the transcurrent plate boundary between the Scotia Plate and the South American Plate (SASPB), with the Magallanes-Fagnano fault system (MFFS, Fig. 1A) representing its western segment (Cunningham et al., 1998; Dalziel et al., 2013; Lodolo et al., 2003, 2002; Ludwig and Rabinowitz, 1982). The NSR extends over a length of about 2000 km from Tierra del Fuego to South Georgia and includes various islands, submarine blocks, and ridges such as the Burdwood Bank (Beniest and Schellart, 2020; Dalziel et al., 2021; Davey, 1972; Nicholson et al., 2020; Riley et al., 2019).

The NSR within the study area is characterized as a Paleozoic-Early Mesozoic basement block with a fold-thrust belt in its northern section (Bry et al., 2004; Ghiglione et al., 2010; Esteban 2014; Esteban et al., 2020). From Lago Fagnano in Tierra del Fuego eastward to 62°W-60°W, the NSR has been interpreted as a releasing bend of the plate boundary (Lodolo et al., 2003; Ghiglione et al., 2010; Esteban, 2014; Ormazabal, 2022). The structures within this release bend are associated with a series of basins aligned along the Magallanes-Fagnano fault system and the NSR that develop above the fold overthrust belt (Esteban et al., 2018; Lodolo et al., 2003).

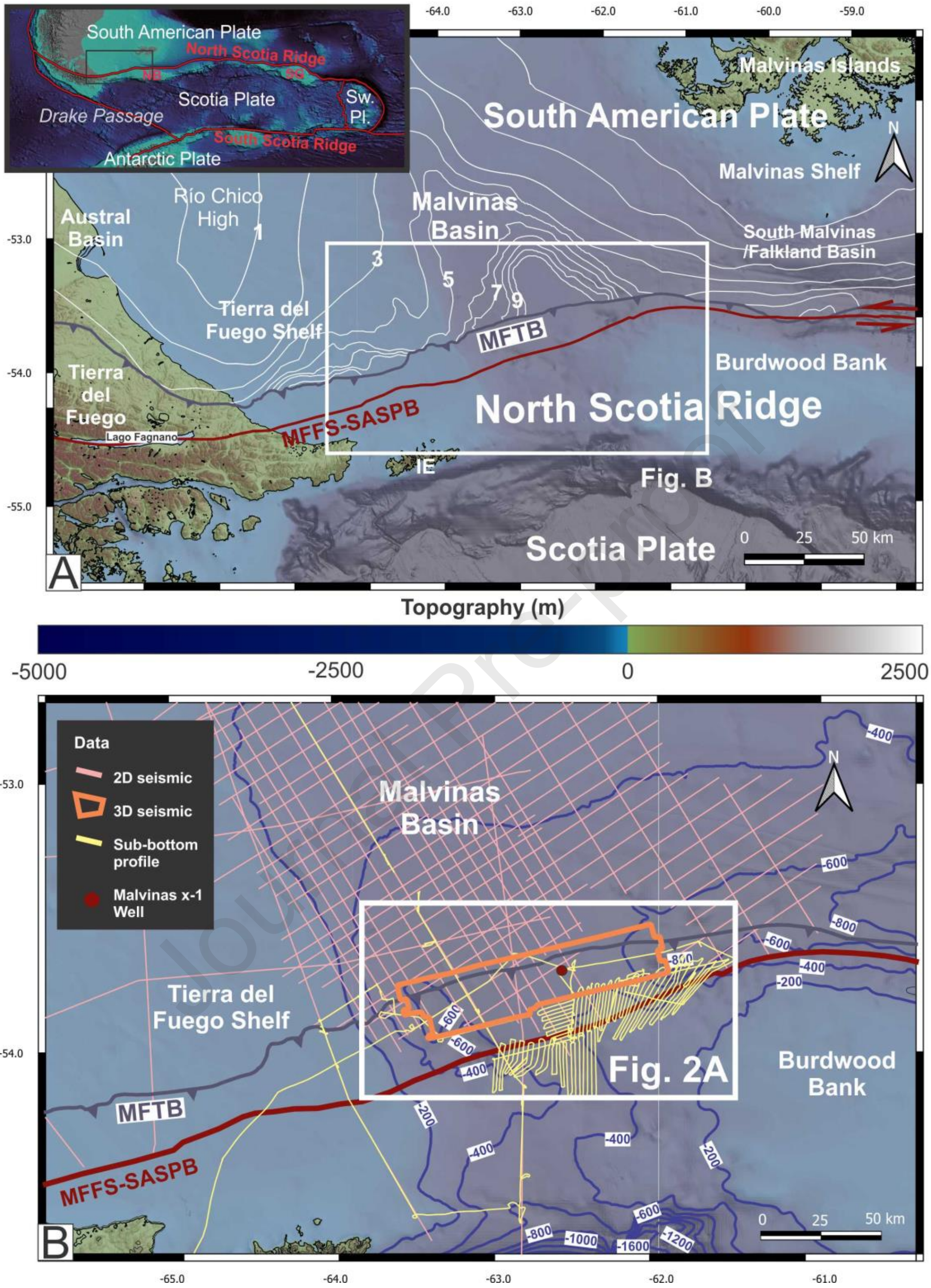

Fig. 1: A: Location of the study region. The blue barbed line indicates the Deformation Front. The dark red line indicates the MFFS-SASPB (Magallanes-Fagnano Fault System-South American-Scotia Plate Boundary). The white lines indicate the sediment thickness (in km) deposited in the basins. BB: Burdwood Bank. SG: South Georgia. Sw. Pl.: Sandwich Plate. IE: Isla de los Estados. MFFS: Magallanes-Fagnano Fault System. SASPB: South American-Scotia Plate Boundary. B: The white rectangle indicates the study area.

The seabed in the southern part of the Malvinas Basin consists of a bathymetric depression with an average depth of 600 m and gentle dips of 1° to 2°, increasing to a depth of 972 m in a contouritic moat (Ormazabal et al., 2024). Seabed depth decreases to the west and north towards the shelves of Tierra del Fuego and the Malvinas Islands, and to the south towards the NSR (Fig. 1B). The transition from the Malvinas Basin to the NSR is accompanied by a flattening of the seabed and the appearance of more chaotic reflections in the seismic lines (Fig. 2C).

2.2 The Malvinas Hydrocarbon Plumbing System

The southern part of the Malvinas Basin and its associated petroleum system have undergone various tectonic phases (Fig. 2; Biddle et al., 1986; Yrigoyen, 1989; Galeazzi, 1998; Tassone et al., 2008; Baristeas et al., 2013; Ormazabal et al., 2019). The first phase of subsidence in the Malvinas Basin began during the Late Triassic (Lovecchio et al., 2019; Uliana et al., 1989) with the rifting of Paleozoic metamorphic units (Tassone et al., 2008; Baristeas et al., 2013) as part of an extensional phase. This phase resulted in the formation of a series of extensional faults (Galeazzi, 1998; Baristeas et al., 2013). After rifting, the region underwent a phase of thermal subsidence during the Cretaceous, which led to the flooding of the basin and the deposition of shales and claystones in the context of an open-neritic regime (Galeazzi, 1998; Tassone et al., 2008; Fig. 2B). These sediments include transgressive deposits of the Springhill Fm. and aggradational layers of the shales of the Lower Inoceramus Fm., which constitute the main source rock of this system (Biddle et al., 1986; DeVito and Kearns, 2022; Galeazzi, 1998).

During the Upper Cretaceous, a significant change in the geodynamic regime of the region resulted in a transition to a compressive/transpressive tectonic mechanism. This phase, known as the Andean orogeny, restructured the Malvinas Basin into a foreland basin system (Fig. 2B; Galeazzi, 1998; Tassone et al., 2008). Consequently, deepening occurred in the southern part of the basin, leading to the entry into the oil window (Galeazzi, 1998; Ghiglione et al., 2010; Baristeas et al., 2013). The sedimentary sequence influenced by this shift spans the period from the latest Cretaceous to the middle Eocene (Tassone et al., 2008; Baristeas et al., 2013).

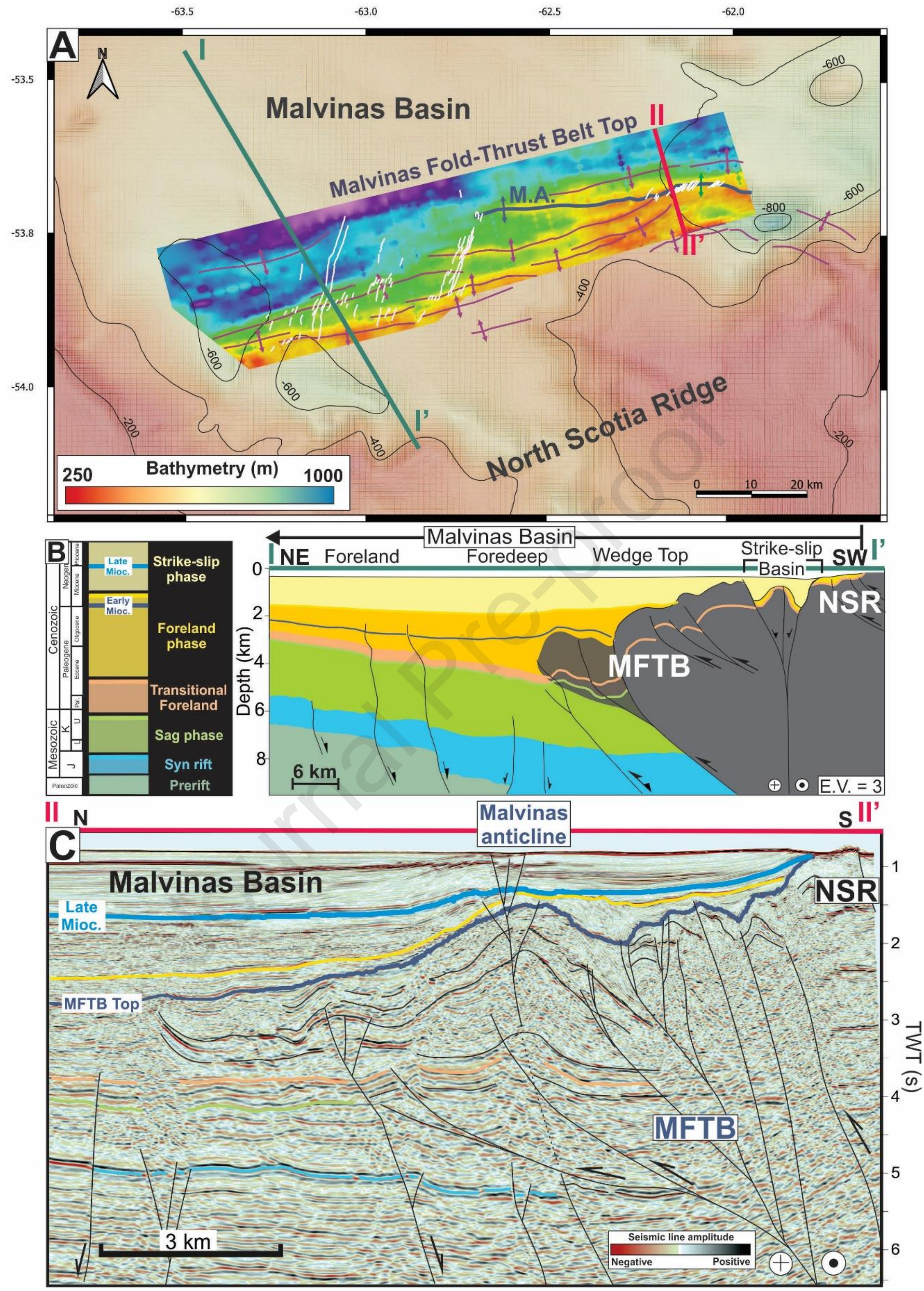

Fig. 2: A: General structure of the Malvinas Fold-Thrust Belt. The hinge of the anticlines are indicated with purple lines. The Malvinas anticline is indicated with a dark blue line. The seabed extensional faults are indicated with white lines. See location in Fig. 1B. B: Seismic units and scheme showing the main unconformities of the southern part of the Malvinas basin, taken from Tassone et al. (2008) and Raggio et al. (2011). C: General configuration of the Malvinas Basin in the study area imaged by a representative multichannel seismic profile. MFTB: Malvinas Fold-Thrust Belt. NSR: North Scotia Ridge.

From the middle Eocene to the early Miocene, another phase of structural deformation occurred in connection with the separation of South America and Antarctica and the opening of the Drake Passage, which led to the formation of the Scotia Plate and the NSR (Barker and Thomas, 2004; Dalziel et al., 2013; Dalziel and Elliot, 1971; Geletti et al., 2005; Ghiglione et al., 2022; Livermore et al., 2005; Lodolo et al., 2006; Maldonado et al., 2014; Tassone et al., 2008). During this phase, the southern deposits in the Malvinas Basin were deformed by the N-NNE-oriented collision between the Tierra del Fuego backstop and the Burdwood Bank with South America (Dalziel et al., 2013; Ghiglione and Cristallini, 2007; Ormazabal et al., 2019; Torres Carbonell et al., 2014). This collision event led to the formation of the MFTB, with hydrocarbon expulsion occurring since at least the Oligocene (Barker, 2001; Cunningham, 1993; Esteban, 2014; Galeazzi, 1998). The deposits associated with this phase in the Malvinas Basin represent wedge-shaped synorogenic units comprising strata up to the Lower Miocene (Tassone et al., 2008).

After the deactivation of the compressional/transpressional pulse, strike-slip tectonics have predominated from the middle Miocene to the present. The onset of strike-slip tectonics in the region is controversial, although there is a general consensus that it became predominant from the late Miocene onwards (Lodolo et al., 2003; Tassone et al., 2008; Ghiglione et al., 2010; Torres Carbonell et al., 2014).

3. Methodology

The dataset used in this work includes 2D and 3D multichannel seismic surveys and sub-bottom acoustic profiles (Fig. 1B, Table 1). Additional information from boreholes was used to correlate the ages determined by these methods with the unconformities recognized in the seismic imaging and acoustic data.

The multichannel seismic reflection data were kindly provided by the Argentine Ministry of Energy and Mining. The 2D seismic data comprise the SPAN, YCM and SWAT97 surveys. The "Malvinas 3-D" dataset consists of 3D seismic data with post-stack time migrated amplitudes, located in the southern part of the Malvinas Basin and the northwesternmost part of the NSR (Fig. 1B). It has a vertical resolution of 14 m (to a maximum depth of 1.5 s two-way travel time; TWT), with an inline spacing of 25 m and a crossline spacing of 12.5 m. The sub-bottom profiles presented in this study were collected using a hull-mounted Parasound P70 echo sounder during the geological-geophysical cruise YTEC-GTGM 1 on board the R/V Austral in 2018, conducted in the southern part of the Malvinas Basin and Burdwood Bank (Fig. 1B).

Method	**Survey**	**Areal extension /Length**	**Max. depth TWT (s)**	**Acquisition Entity**	**Year**
3D Seismic	Malvinas 3D	2300 km^2	9	Western Geco	2005
2D Seismic	SWAT97	2450 km	8	Spectrum Energy	1997
	YCM	6800 km	8	Spectrum Energy	1998
	SPAN	3800 km	16	ION	2009
Sub-bottom Profiler	YTEC-GTGM 1	2613 km	-	IGeBA (UBA-CONICET)/MINDEF	2018

Table 1: Acoustic data used in this study.

The IHS Kingdom Suite software, Version 2017 (https://kingdom.ihs.com/), was utilized to interpret the seismic data, including the calculation of the pseudo-relief volume to support seismic interpretation. The pseudo-relief attribute (Bulhões and de Amorim, 2005) is calculated by applying an inverse Hilbert transform to a user-defined root-mean-square (RMS) amplitude window. The 3D hunt autopicking method within the IHS Kingdom Suite was used to generate high-resolution individual amplitude and time-depth maps for different surfaces, such as the seabed and the top of the MFTB (Fig. 2A).

The stratigraphic framework in this study follows the classification proposed by Tassone et al. (2008). The ages assigned to the Neogene unconformities (Early Miocene, Late Miocene; Fig. 2B) were provided by Raggio et al. (2011) and recognized in the Malvinas x-1 borehole (see Fig. 1B). Correlation between borehole data and seismic data was calibrated with vertical seismic profiles from the well.

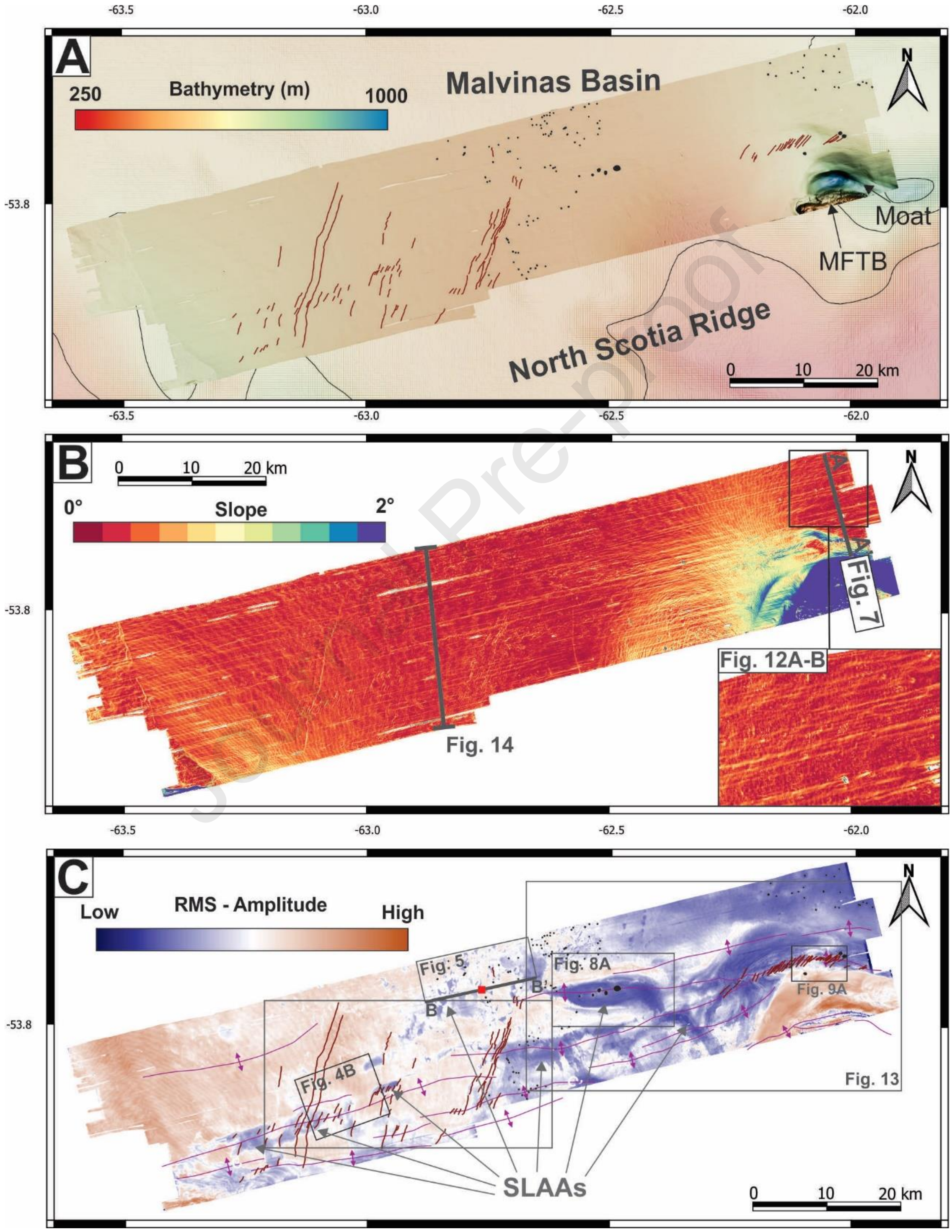

Fig. 3: A: Bathymetry derived from seismic profiles showing the main features recognized in the seabed superposed onto the GEBCO bathymetry. The dark red lines indicate seabed faults. The black dots indicate the fluid seepage

morphologies. MFTB: Malvinas Fold-Thrust Belt B: Slope map and C: Root-mean-square (RMS) Amplitude map of the seabed. SLAAs: Seabed Low Amplitude Anomalies.

The seabed surface was derived from the seismic volume, with depth expressed in s TWT, and converted to meters using an average p-wave velocity of 1500 m/s for the water column. The grid spacing of the seabed surface has the same resolution as the inline and crossline spacing of the seismic volume. Similarly, an RMS amplitude map of the seabed was created. The generation of these amplitude and bathymetric maps from 3D seismic data represents an integrated product of the first few meters of the seabed subsurface (Li et al., 2017; Mosher et al., 2006).

4. Shallow fluid plumbing system characteristics

4.1 Seabed Low Amplitude Anomalies (SLAAs) and enhanced reflectors

The RMS seabed map displays several amplitude features characterized by distinct acoustic responses, with amplitude values anomalously higher or lower than those of the adjacent seabed (Fig. 3C, Fig. 4B). These anomalies vary in size, ranging from several kilometers to less than 100 m, depending on each feature. Most of these anomalies show lower amplitudes compared to the surrounding seabed, hence they are referred to as seabed low-amplitude anomalies (SLAA, Fig. 4B).

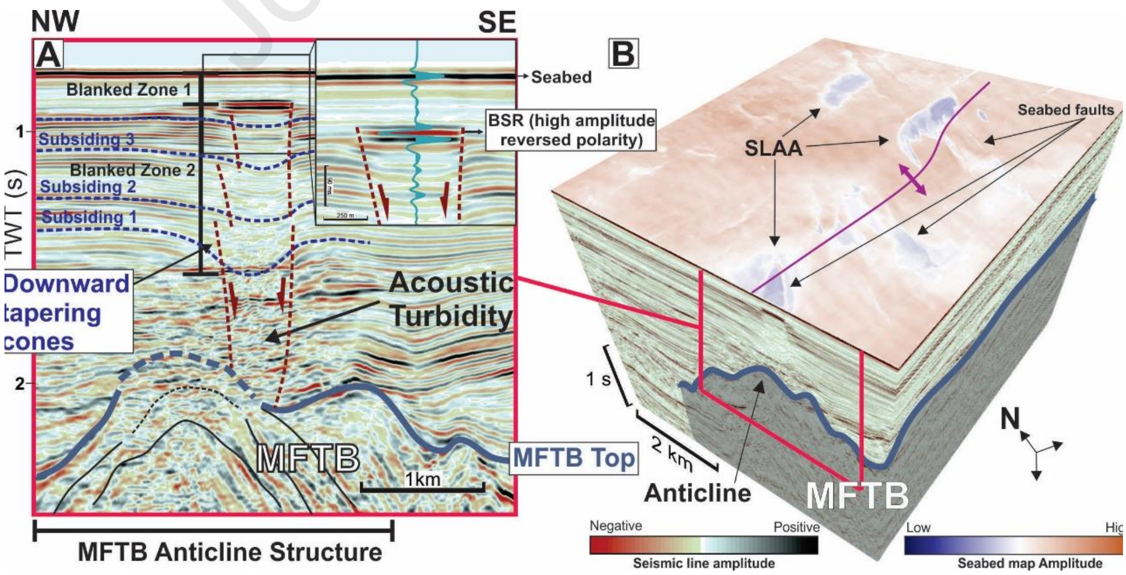

Fig. 4: A: Seismic line showing the acoustic configuration between a SLAA (seabed low-amplitude anomaly) and an anticline of the Malvinas Fold-Thrust Belt. The trace of extensional faults is indicated with dashed dark red lines B:

Root-mean-square amplitude map of the seabed located over an anticline (hinge indicated with a purple line) of the MFTB, indicated with a grey polygon. See location in Fig. 3C.

The SLAAs overlay a distinctive vertical acoustic configuration characterized by a blanked zone between the seabed and a strong reflection with reversed polarity, followed by a second blanked zone below this reflector, overlying a zone with complex imaging (Fig. 4, Fig. 5). In some instances, this configuration is accompanied by acoustic distortion or a wipe-out zone (Fig. 6C). This acoustic configuration consistently appears beneath SLAAs located above the anticlines of the MFTB (Fig. 4). The larger SLAAs, spanning kilometers, are positioned above the hinge of the MFTB anticlines (Fig. 4B). In many of these configurations, the subseabed between the SLAAs and the MFTB shows bicones or downward-tapering cones associated with extensional faults (Fig. 4 and Fig. 6). The enhanced reflections with reversed polarity relative to the seabed are found below the SLAAs at depths between 37 and 168 m below the seabed (assuming a seismic velocity of 1600 m/s; Fig. 5). These reflections mirror the shape of the seabed, particularly being evident when the reflectors have a dipping pattern and intersect the layer reflections (Fig. 7).

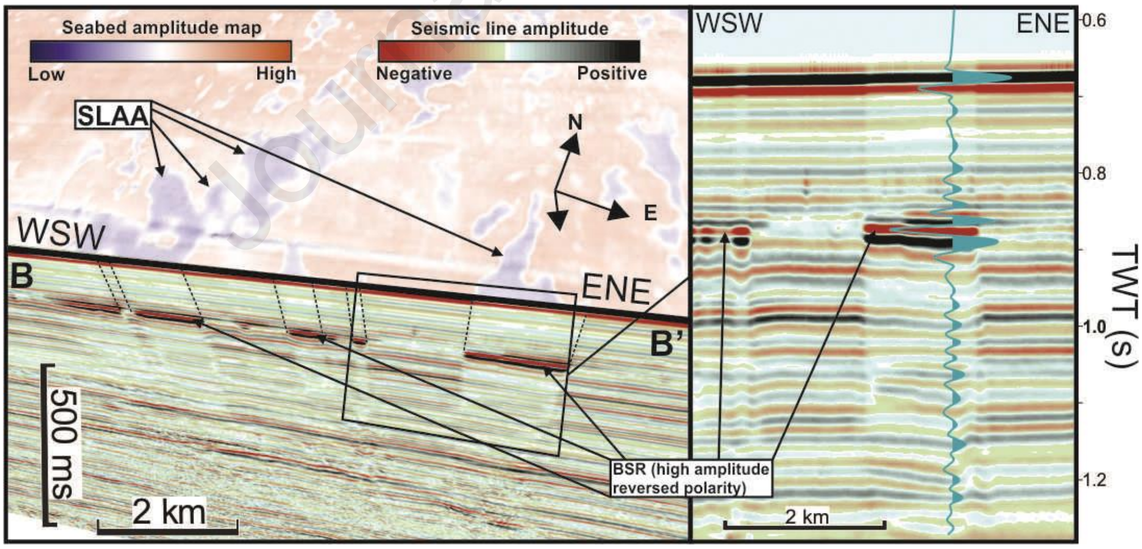

Fig. 5: Seismic profile showing high amplitude reversed polarity, corresponding to a Bottom Simulating Reflector (BSR); superposed to a Root-mean-square amplitude map of the seabed. SLAA: Seabed low amplitude anomaly. See location in Fig. 3C. The location of the green trace is indicated as a red square in the Fig. 3C.

4.1.1 Interpretation

The enhanced reflections with phase reversal are the most striking features in the subseabed below the SLAAs and are here interpreted as the Bottom Simulating Reflector (BSR, Fig. 4), which was observed and calculated in this area by Baristeas et al. (2013) and Gómez et al. (2016). The presence of a BSR usually indicates the base of the gas hydrate stability zone, with sediments below this zone probably saturated with methane (Cox et al., 2021; Reed et al., 1990; Sha et al., 2015; Shedd et al., 2012; Shipley et al., 1979). Baristeas et al. (2013) and Gómez et al. (2016) found that the southern part of the Malvinas Basin has suitable thermodynamic conditions for gas hydrates stability at seabed depths greater than 500 m and demonstrated the existence of a BSR and the gas hydrate stability zone (GHSZ), observed as the blanked zone between the seabed and the BSR (Fig. 4). They rejected a BSR caused by mineralogical transitions or diagenetic effects (Berndt et al., 2004; Hein et al., 1978).

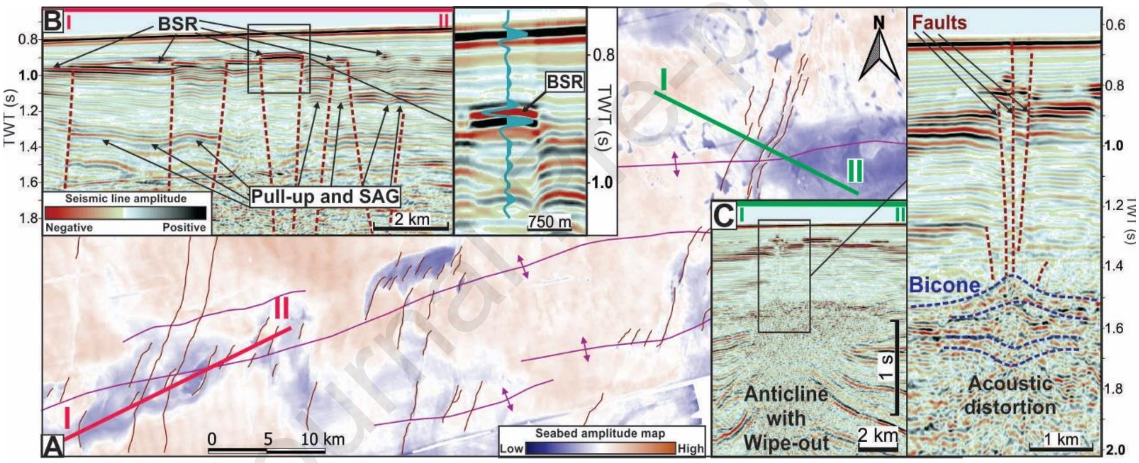

Fig. 6: A: Root-mean-square amplitude map of the seabed showing the trace of the extensional faults indicated with dark red lines. See location in Fig. 3C. B: seismic line showing the displacement produced by these faults (dashed dark red lines) in the subseabed and pull-up and sag acoustic effects, limited by the trace of the faults. Enhanced reflectors with reversed polarity are observed as well, interpreted as Bottom Simulating Reflectors (BSRs). C: seismic line showing a structure of BSRs and enhanced reflectors separating two blanking zones, over an anticline acoustic distortion and wipe-out.

4.2 Pockmarks associated with SLAAs

The largest SLAA feature has an oval shape on the seabed and is located above the Malvinas anticline (Fig. 3C and Fig. 8A). It measures 15 km in an E-W direction and 3.6 km in a N-S direction (Fig. 8A). The hinge of the Malvinas anticline has an intense acoustic distortion, the most significant of the anticlines, which completely masks its inner structure and creates a wipe-out zone below. In this area, the BSR is at its shallowest depth, observable at a depth of only ~37 m below the seabed in the sub-bottom profiles and seismic lines as well (assuming a seismic velocity of 1600 m/s, Fig. 8B-C). The BSR can be observed in the acoustic profiles (SBP) as a stepped pattern of high-amplitude reflections. These reflections overlay an acoustically blanked zone, presumably due to the absorption of the total reflection energy of the SBP acoustic data.

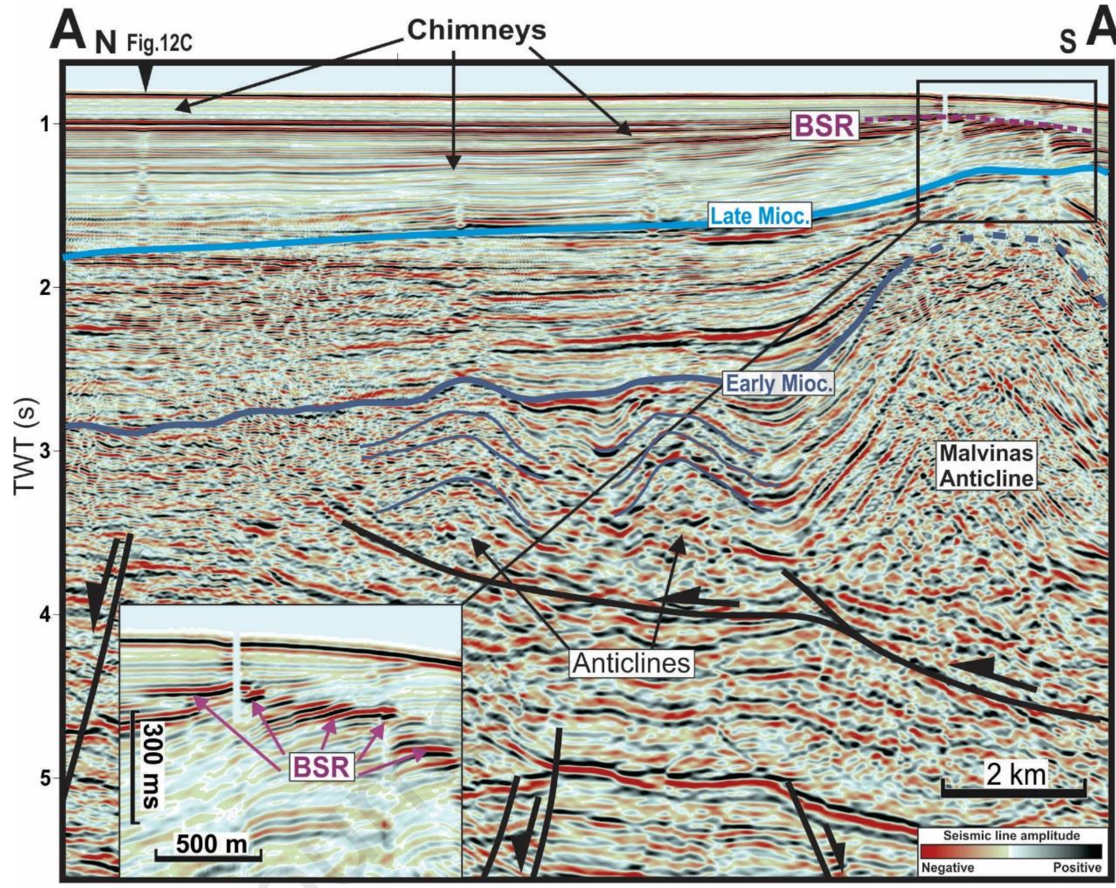

Fig. 7: Seismic line depicting the relationship between the chimneys and the anticlinal structures. See location in Fig. 3B. BSR: Bottom Simulating Reflector.

Five pockmarks are located within the SLAA above the Malvinas anticline, labeled as P1 to P5 in Fig. 8A. These pockmarks can be recognized on the seabed as circular features with high amplitude values, ranging from 300 to 500 m in diameter. Except for pockmark P5, all pockmarks have a low amplitude center. A depression of 1 m is observed in the sub-bottom profile crossing pockmark P4 (assuming a seismic velocity of 1500 m/s, Fig. 8B). Below the depression, a series of U-shaped reflectors can be observed between the seabed and the BSR. These U-shaped reflectors show a progressive increase in diameter with depth, reaching 500 m and a maximum depth of 4 m at 24 m below the seabed.

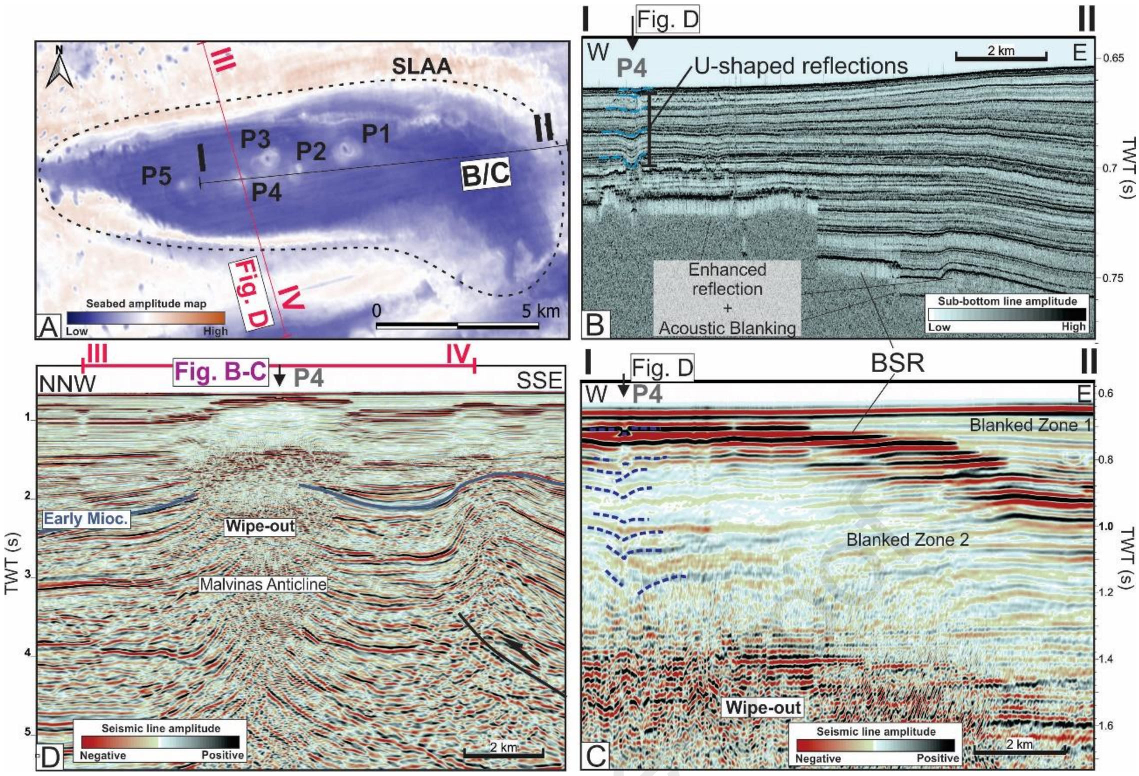

Fig. 8: A: Root-mean-square amplitude map of the seabed showing the largest SLAA (seabed low amplitude anomaly) of the study area, encircled with a dashed black line, located over the Malvinas anticline, indicating the location of pockmarks (P1-P5). See location in Fig. 3C. B: Sub-bottom profile with Pseudo-relief and gaining processing to enhance deeper reflections, located in the same trace than the seismic line of the profile C: Strike seismic line at the same position as the SBP in Fig. 8B. D: Dip seismic section showing the structure of the Malvinas anticline.

4.3 Extensional faults

The seabed amplitude map reveals a series of NE-NNE oriented lineaments with an average length of 1200 m, which can be observed at depth as extensional faults (Fig. 6). The traces of all faults observed on the seabed are associated with high-amplitude anomalies. However, in some cases, they appear as amplitude changes on either side of the faults or as pairs of low and high amplitudes following their position. The position of many of the amplitude anomalies associated with these faults coincide with the larger SLAAs along the anticlinal hinges, particularly in the western half of the study area.

The extensional faults develop above the anticlinal hinges, accompanied by significant acoustic distortions that often obscure the fault structure (Fig. 6C). Most of these faults are distributed in the western half of the 3D seismically surveyed area. A second, smaller group of faults is located in an ENE-WSW band across the hinge of the Malvinas anticline towards the eastern edge of the

3D surveyed area (Fig. 9A). The displacement caused by the faults mainly affects units from anticlinal hinges to units younger than the Late Miocene unconformity (Fig. 9). In many cases, particularly in the eastern part of the study area, the displacement affects younger units, reaching the seabed. Both in the western half of the studied area, as well as over the Malvinas anticline, there are several bicone structures associated with the location of the extensional faults (Fig. 6 and Fig. 10D). In the western part of the studied area, the faults are producing extensional displacement that defines different subsiding areas, associated with downward tapering cones (Fig. 4).

4.3.1 Interpretation

The trace and displacement of the faults are easier to observe in the BSR. Regardless of whether displacement is observed, the trace of the faults to the seabed is associated with several acoustic anomalies, including the BSR as well as a superposition of concave and convex reflections, with the transition from one geometry to the other bounded by the faults. The concave and convex reflections are interpreted as pull-up and sag effects (Fig. 6B).

4.4 Horseshoe mound and pockmarks associated with faults

In the eastern part of the Malvinas anticline, a horseshoe-shaped mound is observed at a water depth of 590 m (Fig. 9B and Fig. 10A). This structure features a central depression, slightly elongated in the N-S direction, surrounded by a horseshoe-shaped ring with a diameter of about 600 m and an opening in the southern part. The ring has a positive relief of about 5 m above the seabed, and the central depression has a depth of 12 m relative to the apex of the ring. The feature shows a higher amplitude than the surrounding seabed, with the amplitude being greatest in the central depression. A pockmark is observed approximately 400 m southeast of the horseshoe mound, consisting of a depression 5 m deep and a diameter of about 600 m, with a higher amplitude than the surrounding seabed (Fig. 9B and Fig. 10A).

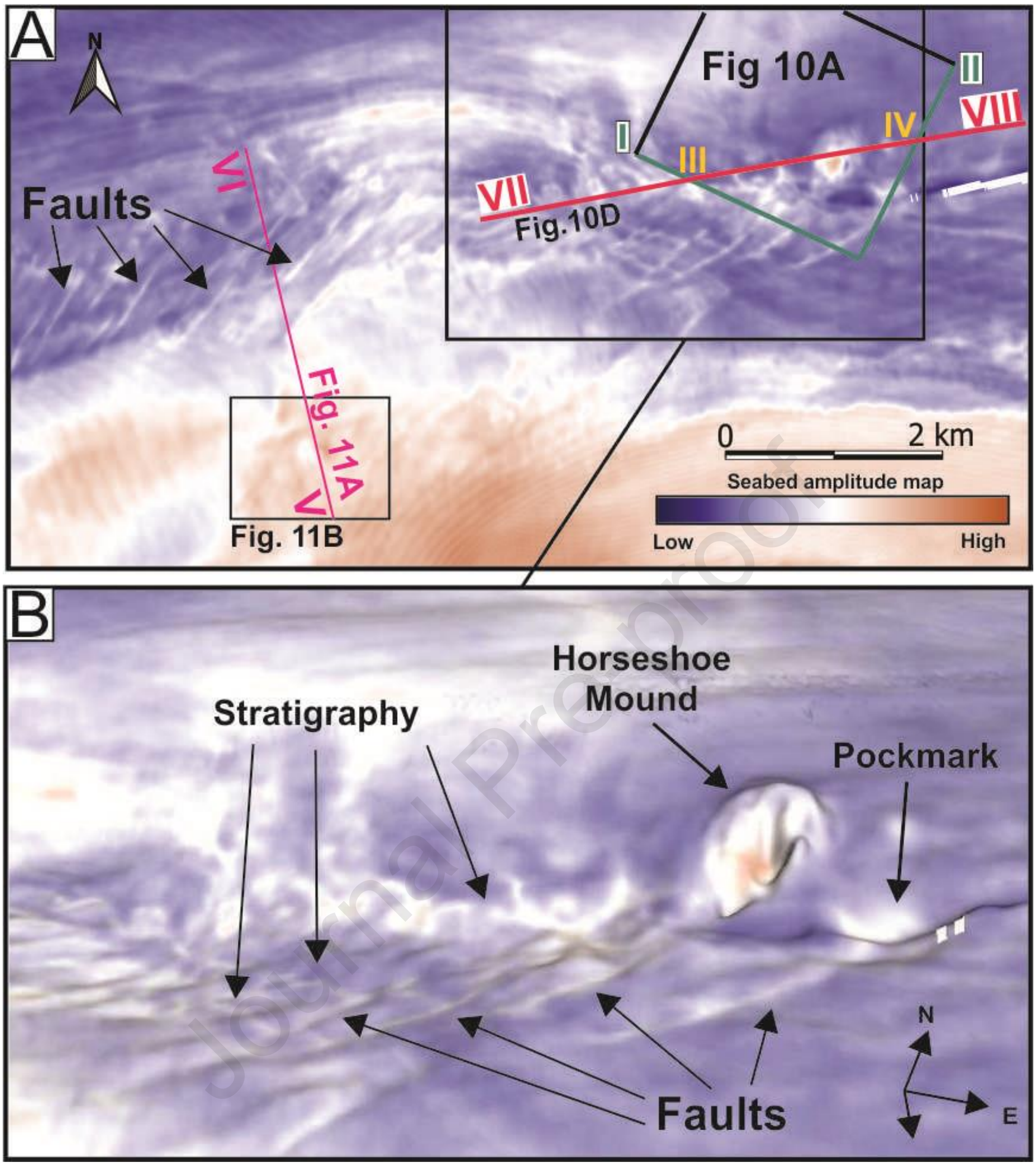

Fig. 9:A: Detail of the Root-mean-square (RMS) amplitude map of the seabed in the eastern part of the study area. See location in Fig. 3C. B: 3D bathymetric map of the seabed with RMS amplitude draped over it.

In the sub-bottom profiles, the subsurface beneath the horseshoe mound appears as a chimney with complete acoustic masking (Fig. 10B-C). The reflections show a distinct change in slope on each side of the chimney, together with some enhanced reflections. The BSR beneath the horseshoe mound and the pockmark is significantly shallower than in the surrounding areas (Fig. 10D). The multichannel seismic shows a certain bicone edifice (Fig. 10D) formed by an upper and a lower bicone. The lower bicone is located in the wipe-out zone. The upper bicone is crossed by a BSR and connected by extensional faults with the lower bicone and the wipe-out zone.

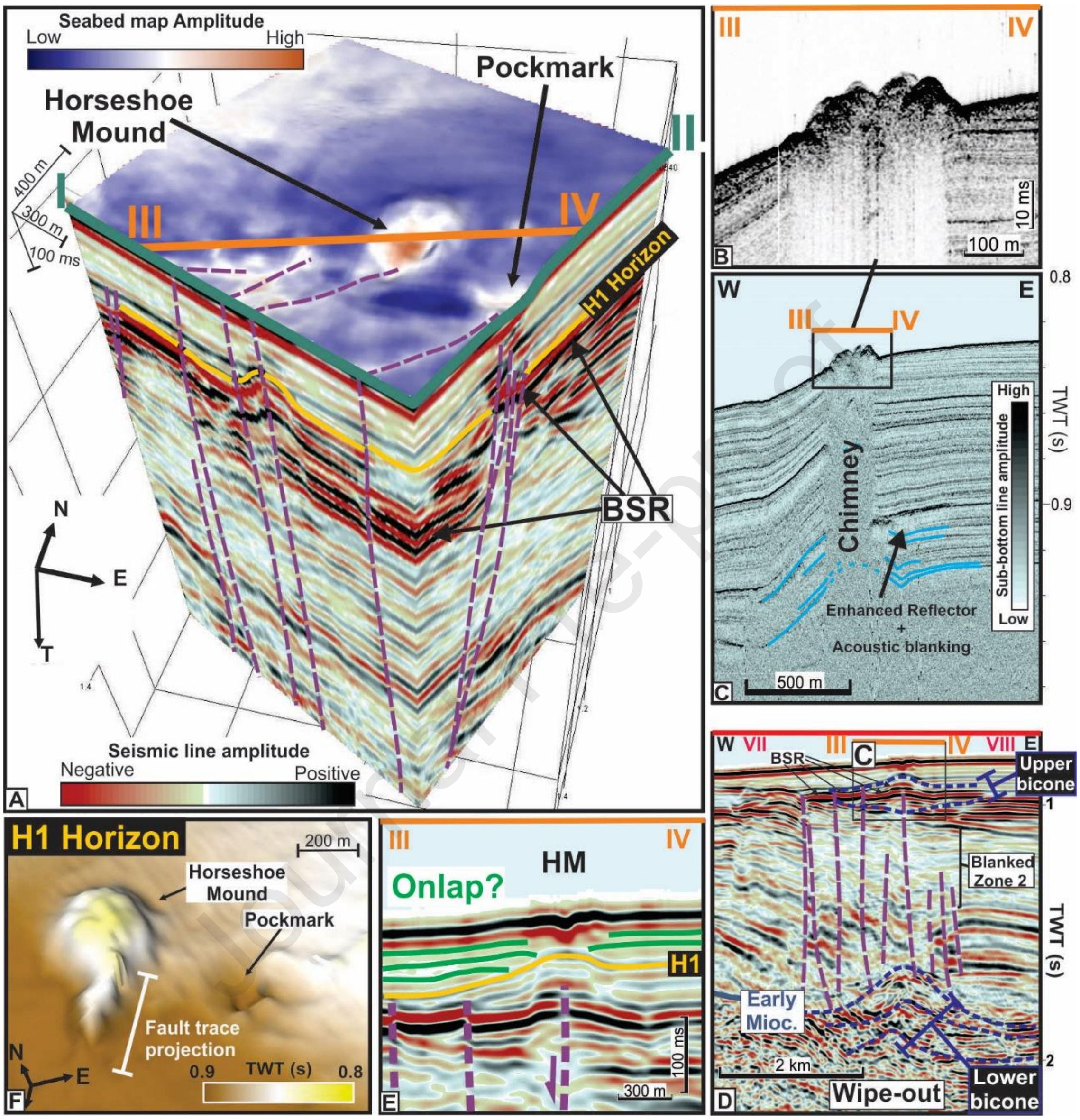

Fig. 10: A: 3D scheme featuring an RMS amplitude map of the seabed and seismic sections in the eastern part of the study area, depicting the horseshoe mound and the neighboring pockmark. These structures are underlain by extensional faults (indicated with purple dashed lines), along with the BSR, shallower just beneath the pockmarks and the horseshoe mound. See location in Fig. 9A. B: Detail of C: Sub-bottom profile showing a chimney located just beneath the horseshoe mound, and the acoustic characteristics of the shallower reflectors associated with the chimney situated below it. D: Seismic line illustrating the acoustic structure underlying the horseshoe mound, depicting two bicones and the faults rooting from the zone with acoustic distortion, causing displacement in the blanked zone 2 and the BSR. See location in Fig. 9A. E: Detail of the seismic section B displaying the reflectors possibly onlapping the Horizon H1, below the horseshoe mound (HM). F: Depth map of the Horizon H1, depicting the domed structure below the horseshoe mound, and a positive structure coinciding with the trace of an extensional fault.

The locations of the horseshoe mound and the adjacent pockmark are related to faults above the Malvinas anticline, that can be observed in the seabed as traces with high-amplitude anomalies (Fig. 9B, Fig. 10A). The displacement of the faults in the seabed is particularly evident in the BSR and the underlying acoustically blanked zone, which is separated from the zone with acoustic distortion by a zone of chaotic multiple reflections of the seabed and the BSR (Fig. 10D-E). The displacement of the faults is observed directly beneath the pockmark and the horseshoe mound as well, with the latter being clearly visible at the depth of the BSR, approximately 46 m below the seabed (assuming a seismic velocity of 1600 m/s, Fig. 10D-E). The first reflections observed beneath the horseshoe mound, including horizon H1, show a domed configuration that mirrors the positive structure along the trace of an extensional fault (Fig. 10A and F). Horizon H1 is partially onlapped by the shallowest subseabed reflectors (Fig. 10E).

A second depression is located 5 km southwest of the horseshoe mound within the Malvinas anticline (Fig. 11). Based on the 3D seismic data, the only information available here, it appears as a pockmark with a 200 m diameter depression filled by the uppermost reflections near the seabed. Below the pockmark, a pipe structure is evidenced, characterized by V- and U-shaped reflections and enhanced reflectors on the sides of the pipe. The pockmark is located near extensional faults on the seabed, although their relationship remains unclear.

4.4.1 Interpretation of the horseshoe mound

The genesis of the horseshoe mound in the eastern part of the Malvinas anticline is inherently associated with extensional faults and acoustic anomalies in the subsurface, specifically the shallow BSR right below it. While the formation of a structure driven by the fluid seepage seems undisputable, the origin of its horseshoe shape could be due to different mechanisms. One possibility for the origin of the structure could be the growth of hydrates in the shallow subsurface, deforming the overlying sediments by forming a hydrate deposit. The hydrate in this deposit can later dissociate and collapse (Hovland and Svensen, 2006; Paull et al., 2008; Serié et al., 2012). Another possibility is the extrusion of fluids or fluidized sediments, constituting a mud volcano (Dimitrov, 2002; Kopf, 2002). In this case, the horseshoe shape would correspond to a center from which the material is extruded, originating the positive structure from the deposition of this material, making it necessary an extrusion of mud or not in order to be classified as a mud volcano.

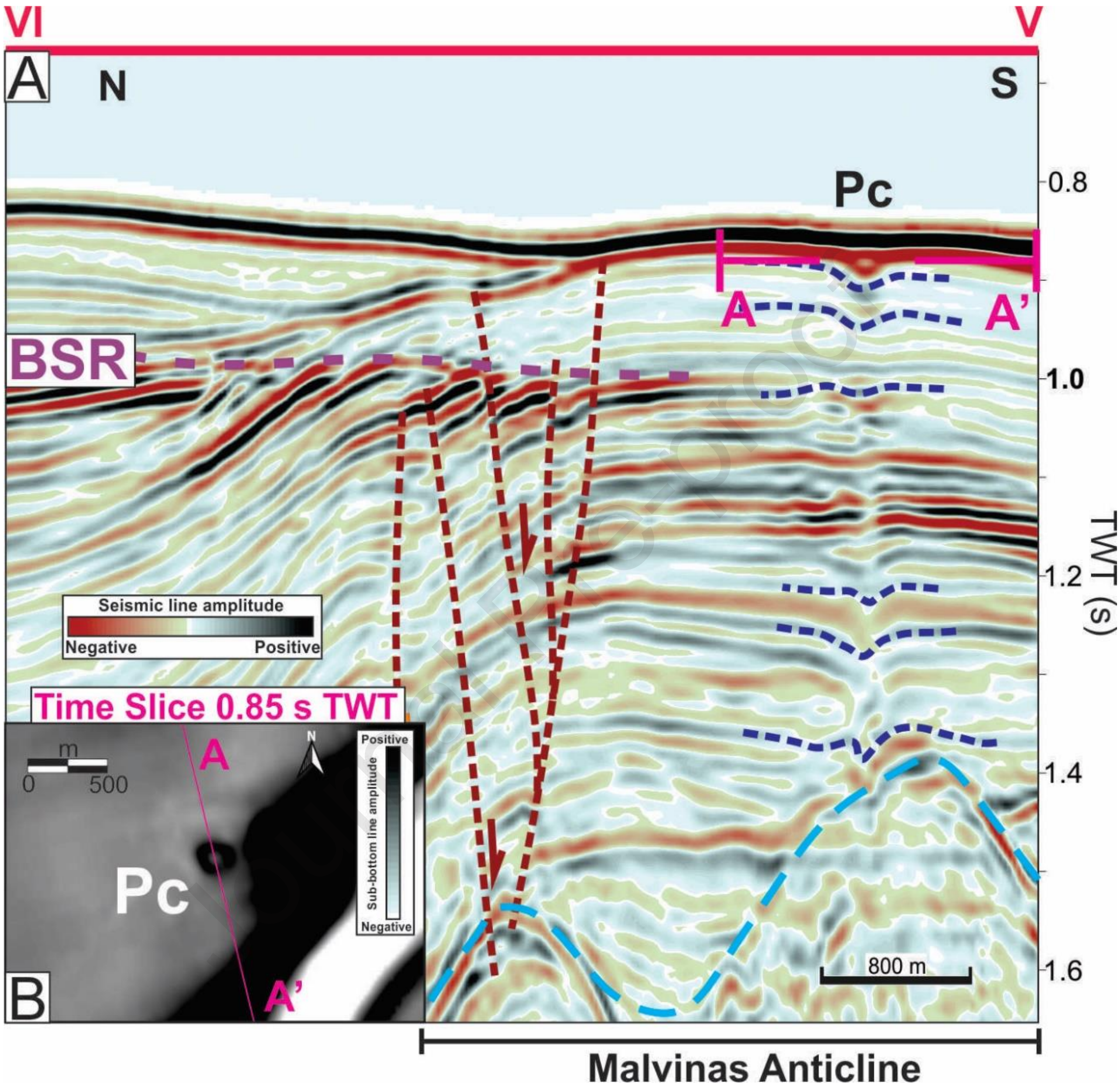

Fig. 11: A: Seismic line showing a pockmark (Pc) associated with a pipe in the southern part of the Malvinas anticline. The Bottom Simulating Reflector (BSR), indicated with purple dashed line, is observed cutting the stratigraphy in the area associated with the extensional faults, indicated with dashed dark red lines. B: Time slice showing the shape of the pockmark in the shallow subseabed. See location in Fig. 9A.

The bulged shape of the reflections beneath the horseshoe mound (e.g., Horizon H1, Fig. 10E-F) indicates either a positive structure or a pull-up effect. The fact that the reflectors adjacent to this bulge from the west appear to onlap the bulge between the BSR and the seabed suggests that the subsurface reflects actual sediment deformation (Fig. 10C). This positive structure in the subseabed, along with its continuation coinciding with the trace of the fault associated with the horseshoe mound, is consistent with material injection through the fault plane. This assertion, along with the absence of structures indicating collapse, suggests that this feature could be classified as a mud volcano. Furthermore, the bicone-shaped volcanic edifice found in the subseabed beneath the horseshoe mound is characteristic of a structure of past mud volcanoes (Sánchez Guillamón et al., 2023; Somoza et al., 2014), implying potential cyclicity in the formation of mud volcanoes in the area. The lower bicone structure within the wipe-out zone appears to have been "disaggregated" by faults and correlates with the Early Miocene reflector that dates the top of the MFTB, similar to what is observed in other compressional belts, such as the giant mud volcanoes in the South Caspian Sea (Davies and Stewart, 2005; Hedayat et al., 2024). However, high-resolution profiles do not reveal any evidence of mud flows on the seabed surrounding the horseshoe mound (Fig. 10B-C). Thus, while the horseshoe mound would be associated with a mud volcanic edifice, it may not represent a mud volcano itself.

Possibly one of the strongest hints on the interpretation of the horseshoe mound, besides its shape, lies in its high reflectivity seafloor, consistent with Methane Derived Authigenic Carbonates (MDACs). The MDACs interpretation is consistent with the underlying mud volcanic structure. MDACs are typically formed by the oxidation of diffuse hydrocarbon flows, similar to those documented in the Gulf of Cadiz, where such positive structures are referred to as carbonate mounds (Akam et al., 2023; Díaz del Río et al., 2003; Magalhães et al., 2012). This carbonate mound likely overlies a buried mud volcano, which may have fed another subsurface mud volcano beneath Horizon H1, contributing to the observed onlap (Fig. 10E, Somoza et al., 2012). Since at present no evidence of mud expulsion is observed on the seafloor, the mound is likely the result of the diffuse migration of hydrocarbons above the younger bicone structure. This migration allows hydrocarbon fluids to be recycled, percolating and oxidizing near the seafloor, forming MDAC pavements. These carbonate mounds are more resistant to erosion, particularly in this region, where strong undercurrents interact with the seafloor (Frey et al., 2021; Nicholson et al., 2020).

4.5 Minimal mounds

Outside the Malvinas anticline, the only seeps observed are minimal mounds on the seabed, so termed because they are about 1 m high. These mounds appear on the seabed amplitude map as sub-circular low amplitude anomalies, without any clear orientation in their distribution (Fig. 3A and Fig. 12A). Many of these features are visible on the seabed as roughly circular mounds less than 1 m high, between 100 and 200 m in diameter, and with a slope of less than 2° (Fig. 12A). Examination of the subsurface reveals that the features between the seabed and the BSR are characterized by minimal bulging of the reflectors (Fig. 12C).

Below the BSR, the reflections show a pattern of stacked U- to V-shaped depressions, accompanied by a reduction in the amplitude of the reflections. This stacked pattern forms continuous chimneys that extend downward to their base. The base of the chimneys is characterized by a zone of acoustic distortion. In some chimneys, this base corresponds to the location of anticlines that lie below the acoustic distortion zone (Fig. 7 and Fig. 12).

4.5.1 Interpretation

The bulging between the seabed and the BSR could represent a positive structure with the same shape of the mounds observed on the seabed. These mounds may represent positive relief on the seabed created by the bulging of shallower units due to gas seeps, similar to the mounds observed over chimneys at various locations (Berndt et al., 2003; Judd and Hovland, 2007; Løseth et al., 2011; Rensbergen et al., 2007; Savini et al., 2009). In the shallow subsurface beneath the mounds, the bulge structure can be observed down to the BSR (Fig. 12). Alternatively, these bulge structures could result from a pull-up effect (Fig. 12C), so they might be interpreted either as a true deformation of the sediment at greater depth due to fluid seepage (Naudts et al., 2006) or as a pull-up effect due to the higher concentration of gas hydrates in the units (Hustoft et al., 2007).

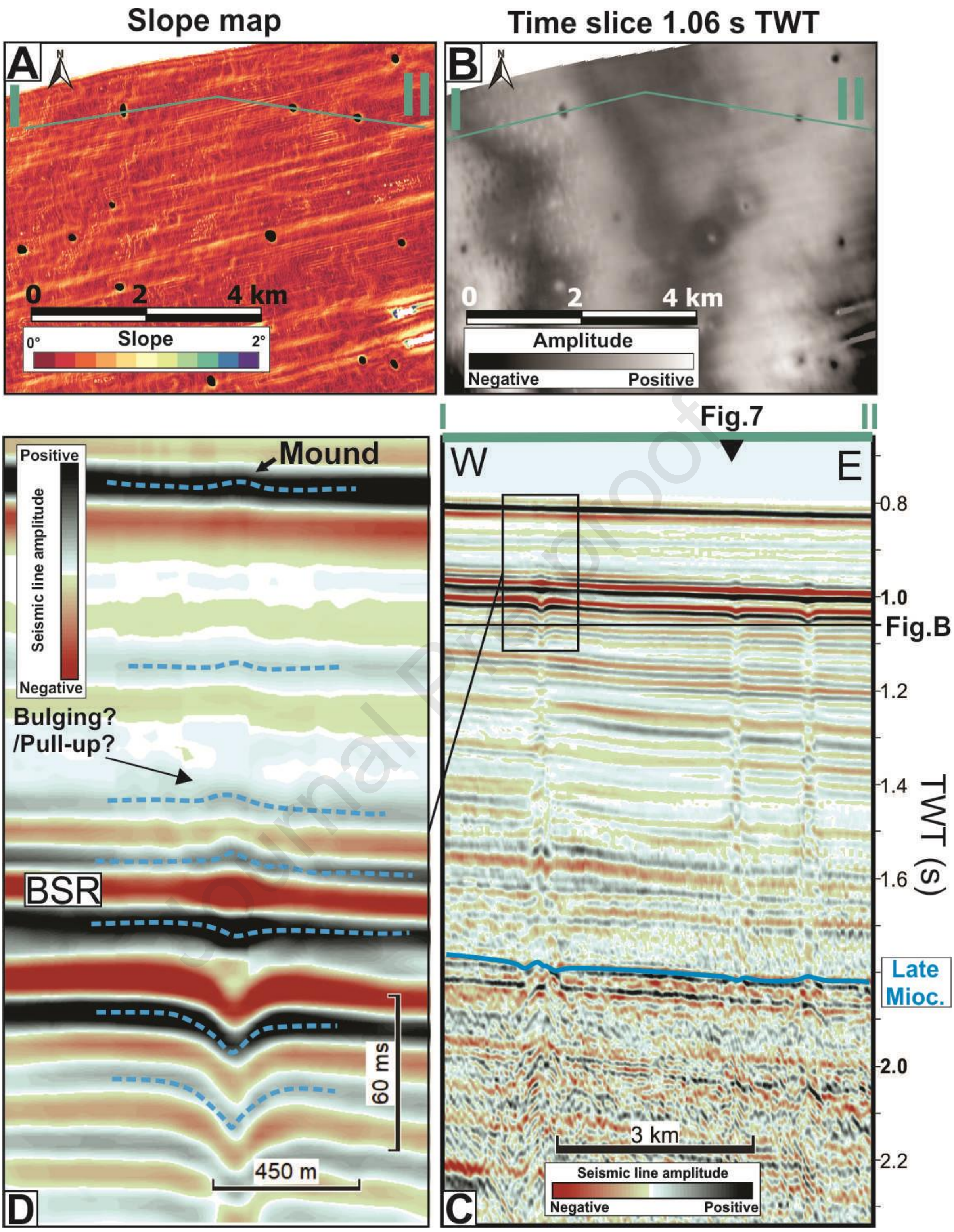

Fig. 12: A: Slope map of the seabed with the minimal mounds indicated by black circles. See location in Fig. 3B. B: Time slice, indicated in C: Seismic line showing the association between chimneys underlying the mounds, as well as D: inset showing the structure of a chimney near the BSR.

Below the BSR/GHSZ, V-shaped depressions in the reflectors forming chimneys beneath the mounds may result from push-down effects, indicating the presence of free gas within the units

(Berndt et al., 2003). The reduction in the amplitude of reflections within the chimneys can also be attributed to the presence of gas in fine sediments (Løseth et al., 2009). The roots of these chimneys are observable in some cases, primarily in areas with acoustic turbidity over anticlines formed from overthrusts of the MFTB and normal faults in the foreland basin (Fig. 7). These discontinuities may have served as conduits that facilitated the migration of the gas (Talukder, 2012).

5. Malvinas plumbing system

Several anticlines in the MFTB underlie SLAAs, and their hinge is characterized by intense acoustic distortion zones, possibly caused by the upwelling of fluids from source rocks (Løseth et al., 2009). Anticlines are known as structures suitable for fluid accumulation (Munn, 1909; Wrather and Lahee, 1934 and references therein). Baristeas et al. (2012) propose a thermodynamic model, attributing the local flattening of the BSR depth above the anticlinal hinges of the MFTB to an increase in the regional geothermal gradient from 23.9 °C/km to a higher local geothermal gradient of 43.5 °C/km induced by the upwelling of high-temperature fluids from source rocks in deeper sectors of the basin (Fig. 8C). This increased geothermal gradient may have led to the emplacement of free gas in the first few meters below the seabed, as indicated by the shallower BSR and the low amplitude anomalies of the seabed, also indicative of shallow free gas (Tóth et al., 2014).

Additionally, based on a dense 2D seismic dataset, Baristeas et al. (2012) concluded that gas of thermogenic origin is present in this area, with hydrocarbons migrating from deep source rocks. This origin is also confirmed by sediment cores (Raggio et al., 2011). The source could correspond to the Springhill and Lower Inoceramus formations (Galeazzi, 1998; Baristeas et al., 2012). In the neighboring South Malvinas/Falkland Basin, Foschi et al. (2019) studied BSR geochemical samples, providing evidence of mature source rocks. Given the equivalent tectonic and stratigraphic settings between the southern part of the Malvinas Basin and the South

Malvinas/Falkland Basin, and the likely shared source rock, this supports the inference of a BSR with thermogenic origin.

The shallow plumbing system likely represents the shallowest part of the proven oil system in the southern part of the Malvinas Basin (Galeazzi, 1998; Raggio et al., 2011; Baristeas et al., 2012). Similar configurations have been observed in various areas associated with gas seeps, including the adjacent South Malvinas/Falkland Basin (Foschi et al., 2019; Foschi and Cartwright, 2016), as well as in other regions worldwide, such as the Niger Delta (Benjamin and Huuse, 2017), the oblique Hikurangi subduction margin off New Zealand (Plaza-Faverola et al., 2014), and several tectonic contexts in the Mediterranean region (Civile et al., 2023; Ferrante et al., 2022; Volpi et al., 2022).

5.1 Gas plumbing system above the Malvinas anticline

The described configuration and interpretation of fluid seepage morphologies in the seabed include pockmarks, a carbonate mound, and minimal mounds (Fig. 3A). Except for the minimal mounds, which do not exceed 200 m in diameter, all the seep morphologies in the seabed are located above the Malvinas anticline (Fig. 13). Furthermore, the largest SLAA is located over the same accumulation structure, indicating a larger amount of fluid presence in the Malvinas anticline compared to other anticlines in the area. Baristeas et al. (2012) identified the largest zone with acoustic distortion in the western part of the Malvinas anticline and interpreted it as a possible mud diapir or the initial stage of the development of a mud volcanic channel.

In the western part of the Malvinas anticline, there are five pockmarks associated with the largest SLAA, whereas the eastern part of the anticline shows a seabed with extensional faults associated with the carbonate mound and two pockmarks. These differences between the western and eastern parts of the anticline suggest slightly different processes of fluid release in the seabed and water column for each sector.

In the western part, the exact timing of pockmarks formation could be related to a significant methane input into the seabed due to a temporary flattening of the BSR and GHSZ (Yang et al., 2021), linked to an increased geothermal gradient caused by the ascent of deep-sourced fluids (Baristeas et al., 2012). The ejection of fluids into the seabed may act as a heat source that increases the geothermal gradient and locally destabilizes and flattens the GHSZ (Chow et al., 2000; Sahling et al., 2009). This flattening of the GHSZ may lead to significant gas dissociation from the hydrates, released into the seabed thereby increasing gas seepage permeability (Bouriak et al., 2000) through pockmarks.

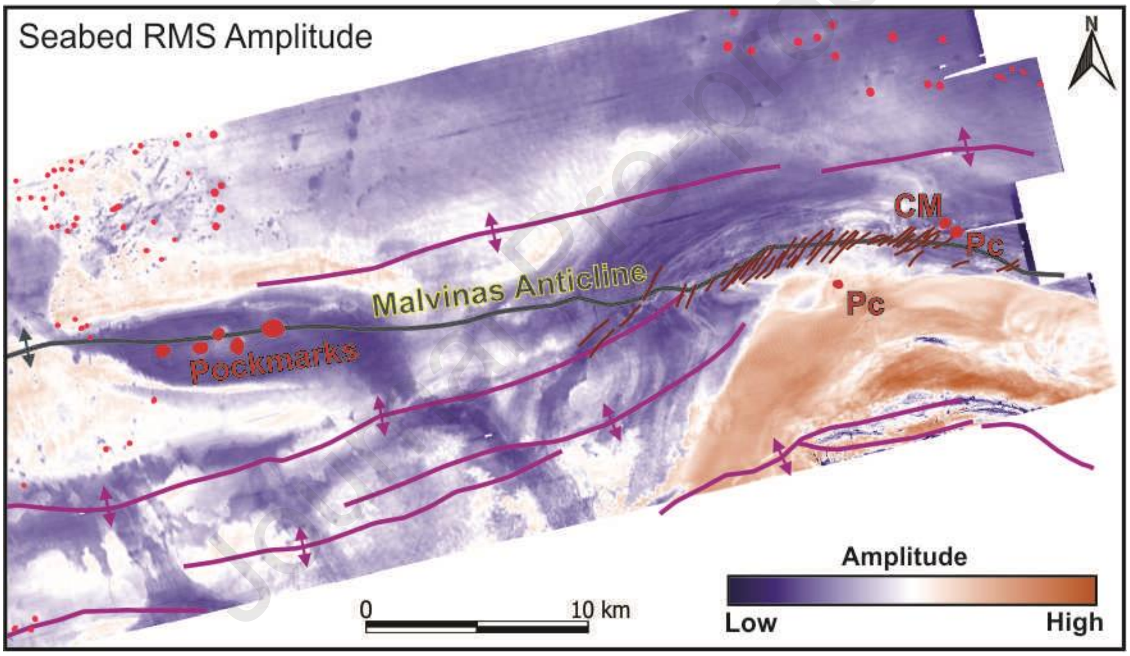

Fig. 13: RMS amplitude map showing the configuration of the largest gas seepage features in the seabed. The hinges of the anticlines of the MFTB are indicated with purple lines. The hinge of the Malvinas anticline is indicated with a dark green line. The seabed extensional faults are indicated with dark red lines. The location of mounds, pockmarks (Pc) and the carbonate mound (CM) are indicated with red polygons. See location in Fig. 3C.

In the eastern part of the Malvinas anticline, the flattening of the associated GHSZ is limited to the location of the carbonate mound and the neighboring pockmark. The existence of this mound may be due to the rise of fluids along extensional faults (Galavazi et al., 2005; Milkov, 2000; Sahling et al., 2008; Van Rensbergen et al., 2005). The role of faults as conduits for the release of fluids at the base of the GHSZ is widely reported in similar tectonic regimes (Conrad et al., 2018; Maloney et al., 2015; Plaza-Faverola and Keiding, 2019).

The carbonate mound and its neighboring pockmark on the Malvinas anticline show a similar evolution: they represent the only features in the Malvinas Basin associated with seabed extensional faults related to transtensional activity (Fig. 9; Ormazabal et al., 2024). In contrast, the other pockmark in the eastern part of the Malvinas anticline, which is not associated with faulting, has different characteristics, including significantly less development, an infilled depression in the seabed, and a dubious relationship with the BSR (Fig. 11).

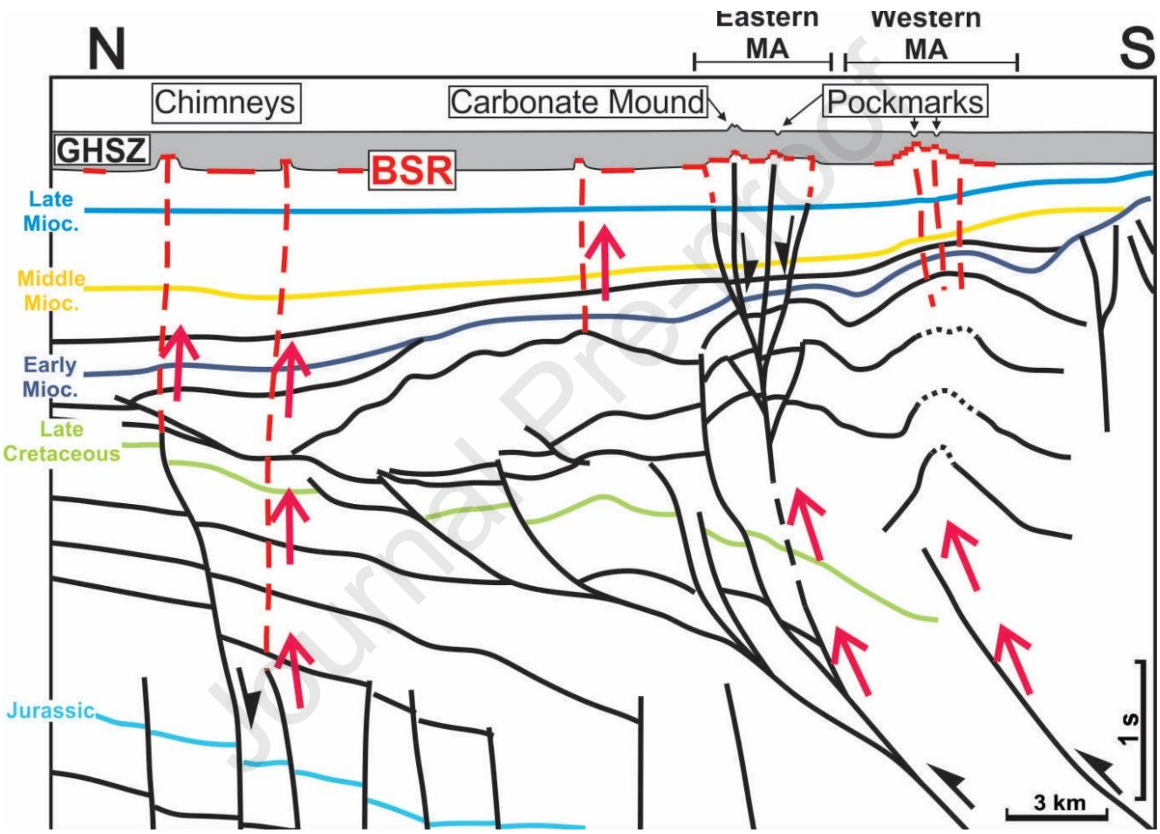

Fig. 14: Conceptual model proposed to explain the migration of fluids from their source to the seabed as pockmarks, chimneys associated with mounds and a mud volcano. The main structure, reflectors and units are derived primarily from a seismic line derived from the 3D seismic volume. See location in Fig. 3B. The Malvinas anticline (MA) was duplicated to represent its migration in its eastern and western parts, incorporating the subseabed configuration, as well as that of the carbonate mound and pockmarks, from Fig. 8D and Fig. 10D.

However, the carbonate mound and pockmark associated with the faults are of the same size as the pockmarks not associated with the faults in the western part of the Malvinas anticline. The similarity of the dimensions of all the features suggests that the presence of faults in the shallow subseabed may have served as conduits for fluid escape, but this is not a necessary condition for fluid escape.

5.2 Dynamics of the Malvinas plumbing system

Given the thermogenic origin (Raggio et al., 2011; Baristeas et al., 2012) of the fluids previously studied in the seabed of the southern part of the Malvinas Basin, their source is identified as the Springhill and Lower Inoceramus formations. These fluids migrated upward from their deep source through extensional faults beneath the orogenic wedge and the overthrusts of the MFTB, accumulating in the anticlines of the MFTB or seeping into the water column (Fig. 14).

One more step in the migration of the fluids seeping to the seafloor could be inferred from the bicones situated above the anticlines of the MFTB (Fig 6C and Fig. 10D). These bicone structures would indicate the occurrence of giant buried mud volcanoes formed by the expulsion of hydrocarbon fluids in response to compression at the front of the MFTB hinges during the opening of the Scotia Sea, which we associate with the diapiric structure interpreted by Baristeas et al. (2012) in the Malvinas anticline. The buried mud volcanoes, developed atop the anticlines, would act afterward as intermediate reservoirs for migrating fluids to the seafloor throughout chimneys and vertical pipes. This migration would explain blanked zones above the buried mud volcanoes. All the chimneys would be formed above the buried mud volcanoes, allowing fluid to migrate to the shallower subsurface as methane hydrates between the seabed and the BSR.

The significant fluid accumulation occurred within the anticlines was sufficient to alter the regional geothermal gradient of the GHSZ, evidenced by the raising of the BSR and SLAAs. This migration, accompanied by increased gas emissions into the seabed, led to the formation of pockmarks in the western part of the Malvinas anticline. In the eastern part of the Malvinas anticline, the NE-oriented extensional faults formed by the current transtensional regime in the seabed served as conduits for fluid leakage, facilitating the formation of the carbonate mound and a pockmark.

The minimal mounds located outside the Malvinas Anticline, indicate the presence of a structure or concentration of gas hydrates associated with the upwelling of fluids from deeper areas. This upwelling is considered necessary to explain these features on the seabed and within the first few meters below. Migration on the seabed outside the anticlines resulted in these chimneys and smaller fluid ejections associated with mounds, with a maximum diameter of 200 m. Such structural hierarchy indicates that the main control on the fluid migration system in this area is exerted by the presence of the MFTB anticlines, with the highest fluid availability occurring in the Malvinas anticline.

6. Conclusions

The Malvinas Basin is a proven hydrocarbon deposit that has not yet been commercially exploited. The large amount of 2D and 3D multichannel seismic profiles acquired over the years and the results of the existing exploration wells have made it possible to outline the potential of this area and identify the most promising geological reservoirs.

The near-surface part of the proven petroleum system in the southern part of the Malvinas Basin has been analyzed here using a series of seismic profiles that reveal a complex plumbing system. It includes a shallow subsurface GHSZ, a discontinuous BSR, as indicated by an analysis of its acoustic signature, and a series of identified faults and gas seeps classified here as pockmarks, a carbonate mound and minimal mounds. The dataset has shown that the main control on the plumbing system in this area is related to the presence of a significant anticlinal structure of the MFTB, which concentrates fluids migrating from deep sources through sub-vertical discontinuities and faults. In areas outside the anticlines, fluid escapes result in scattered and less extensive features, such as minimal mounds. The western part of the Malvinas anticline has five pockmarks, probably formed by a major release of fluids due to a temporary flattening of the GHSZ, suggesting a significant availability of fluids seeping to the seafloor. In the eastern part of the Malvinas anticline, there is a carbonate mound and a pockmark associated with extensional faults that act as conduits for gas seepage to the seabed.

Analysis of the stratigraphy of the area under study suggests that fluids from the Springhill and Lower Inoceramus Formation have migrated to the near-surface depths via extensional faults, some of which underlie the orogenic wedge and overthrusts of the MFTB and have accumulated as methane hydrates in the GHSZ. The anticlines of the MFTB led to greater accumulation, significantly increasing the local geothermal gradient into the GHSZ, indicated by the raised BSR that brings the free gas zone closer to the seabed. Outside the anticlines, there was less fluid release, resulting in chimneys and probably gentle mounds on the seabed.

Due to the non-uniform distribution of available seismic data, it is not yet possible to draw a complete picture of the presence of fluids reaching the surface throughout the southern Malvinas Basin area. However, the analysis presented here provides important information about the dynamics that determine the morphological forms of the seabed. Further studies will be necessary to complete these aspects and, in particular, to plan the sampling of fluids that can provide important clues about the formation and origin of the gas seeps in this region of the south-western Atlantic.

Funding

This research is framed within a collaborative initiative between YPF-Technology (Y-TEC) and the National Scientific and Technical Research Council (CONICET), aimed at coordinating endeavors related to the exploration of the Argentine offshore territory. Furthermore, financial support for this research was provided by the CONICET research project 2021-2023 11220200103152CO (SIMOCA).

Acknowledgments

The authors thank the Argentine Hydrographic Survey (SHN), along with the crew of the R/V Austral and the scientific staff, for their dedicated efforts during the 'YTEC-GTGM 1' cruise. We would like to thank the Argentine Ministry of Energy and Mining for providing us with the 'Malvinas 3D' seismic data utilized in this work. Special recognition is given to Editor-in-Chief Dr.

Qinhong Hu and Section Editor Dr. Tiago Alves for their meaningful feedback. The authors also acknowledge Dr. Luis Somoza, Dr. Marcos Fetter, Dr. Greg Moore, and an anonymous reviewer for their valuable suggestions and comments, which significantly improved the quality of this manuscript.

References

Akam, S.A., Swanner, E.D., Yao, H., Hong, W.L., Peckmann, J., 2023. Methane-derived authigenic carbonates – A case for a globally relevant marine carbonate factory. Earth-Science Rev. 243. https://doi.org/10.1016/j.earscirev.2023.104487

Anka, Z., Loegering, M.J., di Primio, R., Marchal, D., Rodríguez, J.F., Vallejo, E., 2014. Distribution and origin of natural gas leakage in the Colorado Basin, offshore Argentina Margin, South America: seismic interpretation and 3D basin modelling. Geol. Acta 12, 269–285. https://doi.org/10.1344/GeologicaActa2014.12.4.1

Baristeas, N., Anka, Z., di Primio, R., Rodriguez, J.F., Marchal, D., Dominguez, F., 2013. New insights into the tectono-stratigraphic evolution of the Malvinas Basin, offshore of the southernmost Argentinean continental margin. Tectonophysics 604, 280–295. https://doi.org/10.1016/j.tecto.2013.06.009

Baristeas, N., Anka, Z., di Primio, R., Rodriguez, J.F., Marchal, D., Dominguez, F., 2012. Distribution of hydrocarbon leakage indicators in the Malvinas Basin, offshore Argentine continental margin. Mar. Geol. 332–334, 56–74. https://doi.org/10.1016/j.margeo.2012.09.011

Barker, P.F., 2001. Scotia sea regional tectonic evolution: Implications for mantle flow and palaeocirculation, Earth-Science Reviews. https://doi.org/10.1016/S0012-8252(01)00055-1

Barker, P.F., Thomas, E., 2004. Origin, signature and palaeoclimatic influence of the Antarctic

Circumpolar Current. Earth-Science Rev. 66, 143–162. https://doi.org/10.1016/j.earscirev.2003.10.003

Beniest, A., Schellart, W.P., 2020. A geological map of the Scotia Sea area constrained by bathymetry, geological data, geophysical data and seismic tomography models from the deep mantle. Earth-Science Rev. 210, 103391. https://doi.org/10.1016/j.earscirev.2020.103391

Benjamin, U.K., Huuse, M., 2017. Seafloor and buried mounds on the western slope of the Niger Delta. Mar. Pet. Geol. 83, 158–173. https://doi.org/10.1016/j.marpetgeo.2017.02.023

Berndt, C., Bünz, S., Clayton, T., Mienert, J., Saunders, M., 2004. Seismic character of bottom simulating reflectors: Examples from the mid-Norwegian margin. Mar. Pet. Geol. 21, 723–733. https://doi.org/10.1016/j.marpetgeo.2004.02.003

Berndt, C., Bünz, S., Mienert, J., 2003. Polygonal fault systems on the mid-Norwegian margin: A long-term source for fluid flow. Geol. Soc. Spec. Publ. 216, 283–290. https://doi.org/10.1144/GSL.SP.2003.216.01.18

Biddle, K.T., Uliana, M.A., Mitchum, R.M., Fitzgerald, M.G., Wright, R.C., 1986. The stratigraphic and structural evolution of the central and eastern Magallanes Basin, southern South America. Forel. basins 41–61. https://doi.org/10.1002/9781444303810.ch2

Böttner, C., Berndt, C., Reinardy, B.T.I., Geersen, J., Karstens, J., Bull, J.M., Callow, B.J., Lichtschlag, A., Schmidt, M., Elger, J., Schramm, B., Haeckel, M., 2019. Pockmarks in the Witch Ground Basin, Central North Sea. Geochemistry, Geophys. Geosystems 20, 1698–1719. https://doi.org/10.1029/2018GC008068

Bouriak, S., Vanneste, M., Saoutkine, A., 2000. Inferred gas hydrates and clay diapirs near the Storegga Slide on the southern edge of the Voring Plateau, offshore Norway. Mar. Geol. 163, 125–148. https://doi.org/10.1016/S0025-3227(99)00115-2

Bry, M., White, N., Singh, S., England, R., Trowell, C., 2004. Anatomy and formation of oblique continental collision: South Falkland basin. Tectonics 23, 1–20. https://doi.org/10.1029/2002TC001482

Bulhões, É.M., de Amorim, W.N., 2005. Princípio da SismoCamada Elementar e sua aplicação à Técnica Volume de Amplitudes (tecVA), in: 9th International Congress of the Brazilian Geophysical Society & EXPOGEF, Salvador, Bahia, Brazil, 11-14 September 2005.

Ceramicola, S., Dupré, S., Somoza, L., Woodside, J., 2018. Cold Seep Systems, in: Submarine geomorphology. pp. 367–387. https://doi.org/10.1007/978-3-319-57852-1_19

Chen, T.T., Paull, C.K., Liu, C.S., Klaucke, I., Hsu, H.H., Su, C.C., Gwiazda, R., Caress, D.W., 2020. Discovery of numerous pingos and comet-shaped depressions offshore southwestern Taiwan. Geo-Marine Lett. 40, 407–421. https://doi.org/10.1007/s00367-019-00577-z

Chow, J., Lee, J.S., Sun, R., Liu, C.S., Lundberg, N., 2000. Characteristics of the bottom simulating reflectors near mud diapirs: Offshore southwestern Taiwan. Geo-Marine Lett. 20, 3–9. https://doi.org/10.1007/s003670000034

Civile, D., Baradello, L., Accaino, F., Zecchin, M., Lodolo, E., Ferrante, G.M., Markezic, N., Volpi, V., Burca, M., 2023. Fluid-Related Features in the Offshore Sector of the Sciacca Geothermal Field (SW Sicily): The Role of the Lithospheric Sciacca Fault System. Geosciences 13, 231. https://doi.org/10.3390/geosciences13080231

Cole, D., Stewart, S.A., Cartwright, J.A., 2000. Giant irregular pockmark craters in the Palaeogene of the outer Moray Firth Basin, UK North Sea. Mar. Pet. Geol. 17, 563–577. https://doi.org/10.1016/S0264-8172(00)00013-1

Conrad, J.E., Prouty, N.G., Walton, M.A.L., Kluesner, J.W., Maier, K.L., McGann, M., Brothers, D.S., Roland, E.C., Dartnell, P., 2018. Seafloor fluid seeps on Kimki Ridge, offshore southern California: Links to active strike-slip faulting. Deep. Res. Part II Top. Stud. Oceanogr. 150, 82–91. https://doi.org/10.1016/j.dsr2.2017.11.001

Cox, D.R., Huuse, M., Newton, A.M.W., Sarkar, A.D., Knutz, P.C., 2021. Shallow gas and gas hydrate occurrences on the northwest Greenland shelf margin. Mar. Geol. 432, 106382. https://doi.org/10.1016/j.margeo.2020.106382

Cunningham, A.P., Barker, P.F., Tomlinson, J.S., 1998. Tectonics and sedimentary environment of the North Scotia Ridge region revealed by side-scan sonar. J. Geol. Soc. London. 155, 941–956. https://doi.org/10.1144/gsjgs.155.6.0941

Cunningham, W.., 1993. Strike-slip faults in the southernmost andes and the development of the Patagonian orocline. Tectonics 12, 169–186. https://doi.org/10.1029/92TC01790

Dalziel, I.W.D., Elliot, D.H., 1971. Evolution of the scotia arc. Nature 233, 246–252. https://doi.org/10.1038/233246a0

Dalziel, I.W.D., Lawver, L.A., Norton, I.O., Gahagan, L.M., 2013. The Scotia arc: Genesis, evolution, global significance. Annu. Rev. Earth Planet. Sci. 41, 767–793. https://doi.org/10.1146/annurev-earth-050212-124155

Dalziel, I.W.D., Macdonald, D.I.M., Stone, P., Storey, B.C., 2021. South Georgia microcontinent: Displaced fragment of the southernmost Andes. Earth-Science Rev. 220, 103671. https://doi.org/10.1016/j.earscirev.2021.103671

Davey, F.J., 1972. Gravity measurements over Burdwood Bank. Mar. Geophys. Res. 1, 428–435.

Davies, R.J., Stewart, S.A., 2005. Emplacement of giant mud volcanoes in the South Caspian Basin: 3D seismic reflection imaging of their root zones. J. Geol. Soc. London. 162, 1–4. https://doi.org/10.1144/0016-764904-082

DeVito, S., Kearns, H., 2022. Overview of the exploration potential of offshore Argentina – insight from new seismic interpretations. Pet. Geosci. 28. https://doi.org/10.1144/petgeo2020-

132

Díaz del Río, V., Somoza, L., Martínez-Frias, J., Mata, M.P., Delgado, A., Hernandez-Molina, F., Lunar, R., Martín-Rubí, J.A., Maestro, A., Fernández-Puga, M.C., León, R., Llave, E., Medialdea, T., Vázquez, J.T., 2003. Vast fields of hydrocarbon-derived carbonate chimneys related to the accretionary wedge/olistostrome of the Gulf of Cádiz. Mar. Geol. 195, 177–200. https://doi.org/10.1016/S0025-3227(02)00687-4

Dimitrov, L.I., 2002. Mud volcanoes-the most important pathway for degassing deeply buried sediments. Earth-Science Rev. 59, 49–76. https://doi.org/10.1016/S0012-8252(02)00069-7

Esteban, F.D., 2014. Estudio geofísico-geológico del subsuelo del segmento noroccidental de la Dorsal Norte de Scotia. Argentina. Unpublished PhD thesis, University of Buenos Aires.

Esteban, F.D., Ormazabal, J.P., Palma, F., Cayo, L.E., Lodolo, E., Tassone, A., 2020. Strike-slip related folding within the Malvinas/Falkland Trough (south-western Atlantic ocean). J. South Am. Earth Sci. 98, 102452. https://doi.org/10.1016/j.jsames.2019.102452

Esteban, F.D., Tassone, A., Isola, J.I., Lodolo, E., Menichetti, M., 2018. Geometry and structure of the pull-apart basins developed along the western South American-Scotia plate boundary (SW Atlantic Ocean). J. South Am. Earth Sci. 83, 96–116. https://doi.org/10.1016/j.jsames.2018.02.005

Ferrante, G.M., Accaino, F., Civile, D., Lodolo, E., Volpi, V., Romeo, R., Accettella, D., 2022. Deep and shallow gas occurrence in the NW Sicilian Channel and related features. Mar. Pet. Geol. 139, 105575. https://doi.org/10.1016/j.marpetgeo.2022.105575

Foschi, M., Cartwright, J.A., 2016. South Malvinas/Falkland Basin: Hydrocarbon migration and petroleum system. Mar. Pet. Geol. 77, 124–140. https://doi.org/10.1016/j.marpetgeo.2016.06.002

Foschi, M., Paganoni, M., Cartwright, J.A., Idiz, E., 2019. Microbial vs thermogenic gas hydrates in the South Falkland Basin: BSR distribution and fluid origin. Mar. Pet. Geol. 102, 695–703. https://doi.org/10.1016/j.marpetgeo.2019.01.023

Frey, D.I., Piola, A.R., Krechik, V.A., Fofanov, D. V., Morozov, E.G., Silvestrova, K.P., Tarakanov, R.Y., Gladyshev, S. V., 2021. Direct Measurements of the Malvinas Current Velocity Structure. J. Geophys. Res. Ocean. 126. https://doi.org/10.1029/2020JC016727

Galavazi, M., Wegerif, J., Razak, Z., Hamilton, I., 2005. Beating Caspian geohazards, Block 1 development, Turkmenistan. Proc. Annu. Offshore Technol. Conf. 2005-May, 1017–1022. https://doi.org/10.4043/17360-ms

Galeazzi, J.S., 1998. Structural and Stratigraphic Evolution of the Western Malvinas Basin, Argentina. Am. Assoc. Pet. Geol. Bull. 82, 596–636.

Gay, A., Lopez, M., Berndt, C., Séranne, M., 2007. Geological controls on focused fluid flow associated with seafloor seeps in the Lower Congo Basin. Mar. Geol. 244, 68–92. https://doi.org/10.1016/j.margeo.2007.06.003

Gay, A., Lopez, M., Cochonat, P., Séranne, M., Levaché, D., Sermondadaz, G., 2006. Isolated seafloor pockmarks linked to BSRs, fluid chimneys, polygonal faults and stacked Oligocene-Miocene turbiditic palaeochannels in the Lower Congo Basin. Mar. Geol. 226, 25–40. https://doi.org/10.1016/j.margeo.2005.09.018

Geletti, R., Lodolo, E., Schreider, A.A., Polonia, A., 2005. Seismic structure and tectonics of the Shackleton Fracture Zone (Drake Passage, Scotia Sea). Mar. Geophys. Res. 26, 17–28. https://doi.org/10.1007/s11001-005-0147-4

Ghiglione, M.C., Cristallini, E.O., 2007. Have the southernmost Andes been curved since Late Cretaceous time? An analog test for the Patagonian Orocline. Geology 35, 13–16. https://doi.org/10.1130/G22770A.1

Ghiglione, M.C., Gallardo-Jara, R., Albano, J., Kress, P., Raggio, F., 2022. Depocentros Cenozocios de la Cuenca Austral en el contexto de la apertura del Pasaje de Drake, in: 11° Congreso de Exploración y Desarrollo de Hidrocarburos CONEXPLO.

Ghiglione, Matías C, Quinteros, J., Yagupsky, D., Bonillo-martínez, P., Hlebszevtich, J., Ramos, V.A., Vergani, G., Figueroa, D., 2010. Journal of South American Earth Sciences Structure and tectonic history of the foreland basins of southernmost South America. J. South Am. Earth Sci. 29, 262–277. https://doi.org/10.1016/j.jsames.2009.07.006

Gómez, J.L., Späth, F.G.E., Pianelli, L., 2016. Evidencias sísmicas de hidratos de gas y cuantificación de su potencial económico en el mar Argentino, cuenca de malvinas. Geoacta 41, 35–49.

Hedayat, B., Soleimani Monfared, M., Losada, L.S., 2024. Automatic mud diapir detection using ANFIS expert systems algorithm; a case study in the Gorgan plain, Iran. Environ. Earth Sci. 83, 403. https://doi.org/10.1007/s12665-024-11703-1

Hein, J.R., Scholl, D.W., Barron, J.A., Jones, M.G., Miller, J., 1978. Diagenesis of late Cenozoic diatomaceous deposits and formation of the bottom simulating reflector in the southern Bering Sea. Sedimentology 25, 155–181. https://doi.org/10.1111/j.1365-3091.1978.tb00307.x

Hovland, M., Judd., A.G., 1988. Seabed Pockmark and Seepage: Impact on Geology, Biology and the Marine Environment. https://doi.org/10.13140/RG.2.1.1414.1286

Hovland, M., Svensen, H., 2006. Submarine pingoes: Indicators of shallow gas hydrates in a pockmark at Nyegga, Norwegian Sea. Mar. Geol. 228, 15–23. https://doi.org/10.1016/j.margeo.2005.12.005

Hustoft, S., Mienert, J., Bünz, S., Nouzé, H., 2007. High-resolution 3D-seismic data indicate focussed fluid migration pathways above polygonal fault systems of the mid-Norwegian margin. Mar. Geol. 245, 89–106. https://doi.org/10.1016/j.margeo.2007.07.004

Idczak, J., Brodecka-Goluch, A., Łukawska-Matuszewska, K., Graca, B., Gorska, N., Klusek, Z., Pezacki, P.D., Bolałek, J., 2020. A geophysical, geochemical and microbiological study of a newly discovered pockmark with active gas seepage and submarine groundwater discharge (MET1-BH, central Gulf of Gdańsk, southern Baltic Sea). Sci. Total Environ. 742. https://doi.org/10.1016/j.scitotenv.2020.140306

Isola, J.I., Bravo, M.E., Bozzano, G., Palma, F.I., Ormazabal, J.P., Principi, S., Spoltore, D., Martin, R., Esteban, F.D., Tassone, A.A., 2021. The Late-Quaternary deposits of the Piedra Buena Terrace (Patagonian continental slope, SW Atlantic): An example of interaction between bottom currents and seafloor morphology. Mar. Geol. 435, 106459. https://doi.org/10.1016/j.margeo.2021.106459

Isola, J.I., Ormazabal, J.P., Flores, G., Arismendi, S., Druet, M., Muñoz, A., Río, J.L. de., Etienot, S.D.A., Gomez Ballesteros, M.P., Principi, S., Bolatti, N.D., Tassone, A.A., 2020. Tectonic and structural controls on Neogene fluid release in the Patagonian Continental Margin. Mar. Pet. Geol. 115, 104246. https://doi.org/10.1016/j.marpetgeo.2020.104246

Judd, A., Hovland, M., 2007. Seabed Fluid Flow. Cambridge University Press. https://doi.org/10.1017/CBO9780511535918

Kennedy, B.R.C., Rotjan, R.D., 2023. Mind the gap: comparing exploration effort with global biodiversity patterns and climate projections to determine ocean areas with greatest exploration needs. Front. Mar. Sci. 10, 1–10. https://doi.org/10.3389/fmars.2023.1219799

Kim, Y.G., Kim, S., Lee, D.H., Lee, Y.M., Kim, H.J., Kang, S.G., Jin, Y.K., 2020. Occurrence of active gas hydrate mounds in the southwestern slope of the Chukchi Plateau, Arctic Ocean. Episodes 43, 811–823. https://doi.org/10.18814/EPIIUGS/2020/020053

Kopf, A.J., 2002. Significance of mud volcanism. Rev. Geophys. 40, 2-1-2–52.

https://doi.org/10.1029/2000RG000093

Kunath, P., Crutchley, G., Chi, W.C., Berndt, C., Liu, C.S., Elger, J., Klaeschen, D., Bohrmann, G., 2022. Episodic Venting of a Submarine Gas Seep on Geological Time Scales: Formosa Ridge, Northern South China Sea. J. Geophys. Res. Solid Earth 127. https://doi.org/10.1029/2022JB024668

Kvenvolden, K.A., Barnard, L.A., 1983. Hydrates of natural gas in continental margins. Stud. Cont. margin Geol. 34, 631–640.

Li, X., Liu, B., Liu, L., Zheng, J., Zhou, S., Zhou, Q., 2017. Prediction for potential landslide zones using seismic amplitude in Liwan gas field, northern South China Sea. J. Ocean Univ. China 16, 1035–1042. https://doi.org/10.1007/s11802-017-3308-6

Livermore, R., Nankivell, A., Eagles, G., Morris, P., 2005. Paleogene opening of Drake Passage. Earth Planet. Sci. Lett. 236, 459–470. https://doi.org/10.1016/j.epsl.2005.03.027

Lodolo, E., Donda, F., Tassone, A., 2006. Western Scotia Sea margins: Improved constraints on the opening of the Drake Passage. J. Geophys. Res. Solid Earth 111, 1–14. https://doi.org/10.1029/2006JB004361

Lodolo, E., Menichetti, M., Bartole, R., Ben-Avraham, Z., Tassone, A., Lippai, H., 2003. Magallanes-Fagnano continental transform fault (Tierra del Fuego, southernmost South America). Tectonics 22. https://doi.org/10.1029/2003tc001500

Lodolo, E., Menichetti, M., Tassone, A., Geletti, R., Sterzai, P., Lippai, H., Hormaechea, J.L., 2002. Researchers target a continental transform fault in tierra del fuego. Eos (Washington. DC). 83. https://doi.org/10.1029/2002EO000001

Løseth, H., Gading, M., Wensaas, L., 2009. Hydrocarbon leakage interpreted on seismic data. Mar. Pet. Geol. 26, 1304–1319. https://doi.org/10.1016/j.marpetgeo.2008.09.008

Løseth, H., Wensaas, L., Arntsen, B., Hanken, N.M., Basire, C., Graue, K., 2011. 1000 M Long Gas Blow-Out Pipes. Mar. Pet. Geol. 28, 1047–1060. https://doi.org/10.1016/j.marpetgeo.2010.10.001

Lovecchio, J.P., Naipauer, M., Cayo, L.E., Rohais, S., Giunta, D., Flores, G., Gerster, R., Bolatti, N.D., Joseph, P., Valencia, V.A., Ramos, V.A., 2019. Rifting evolution of the Malvinas basin, offshore Argentina: New constrains from zircon U–Pb geochronology and seismic characterization. J. South Am. Earth Sci. 95, 102253. https://doi.org/10.1016/j.jsames.2019.102253

Ludwig, W.J., Rabinowitz, P.D., 1982. The collison complex of the North Scotia ridge. J. Geophys. Res. 87, 3731–3740. https://doi.org/10.1029/JB087iB05p03731

Ma, G., Zhan, L., Lu, H., Hou, G., 2021. Structures in Shallow Marine Sediments Associated with Gas and Fluid Migration. J. Mar. Sci. Eng. 9, 396. https://doi.org/10.3390/jmse9040396

Magalhães, V.H., Pinheiro, L.M., Ivanov, M.K., Kozlova, E., Blinova, V., Kolganova, J., Vasconcelos, C., McKenzie, J.A., Bernasconi, S.M., Kopf, A.J., Díaz-del-Río, V., González, F.J., Somoza, L., 2012. Formation processes of methane-derived authigenic carbonates from the Gulf of Cadiz. Sediment. Geol. 243–244, 155–168. https://doi.org/10.1016/j.sedgeo.2011.10.013

Maldonado, A., Bohoyo, F., Galindo-Zaldívar, J., Hernández-Molina, F.J., Lobo, F.J., Lodolo, E., Martos, Y.M., Pérez, L.F., Schreider, A.A., Somoza, L., 2014. A model of oceanic development by ridge jumping: Opening of the Scotia Sea. Glob. Planet. Change 123, 152–173. https://doi.org/10.1016/j.gloplacha.2014.06.010

Maloney, J.M., Grupe, B.M., Pasulka, A.L., Dawson, K.S., Case, D.H., Frieder, C.A., Levin, L.A., Driscoll, N.W., 2015. Transpressional segment boundaries in strike-slip fault systems offshore southern California: Implications for fluid expulsion and cold seep habitats. Geophys. Res. Lett. 42, 4080–4088. https://doi.org/10.1002/2015GL063778

Milkov, A. V., 2000. Worldwide distribution of submarine mud volcanoes and associated gas hydrates. Mar. Geol. 167, 29–42. https://doi.org/10.1016/S0025-3227(00)00022-0

Mordukhovich, V. V., Krylova, E.M., Dando, P.R., 2023. Seeps and vents of the Bering Sea. Deep Sea Res. Part II Top. Stud. Oceanogr. 209, 105290. https://doi.org/10.1016/j.dsr2.2023.105290

Mosher, D., Bigg, S., LaPierre, A., 2006. 3D seismic versus multibeam sonar seafloor surface renderings for geohazard assessment: Case examples from the central Scotian Slope. Lead. Edge 25, 1484–1494. https://doi.org/10.1190/1.2405334

Munn, M.J., 1909. The anticlinal and hydraulic theories of oil and gas accumulation. Econ. Geol. 4, 5059–529.

Muñoz, A., Cristobo, J., Rios, P., Druet, M., Polonio, V., Uchupi, E., Acosta, J., Iglesias, S., Portela, J., del Río, J.L., Parra, S., Sacau, M., Vilela, R., Patrocinio, T., Almón, B., Elvira, E., Jiménez, P., Fontán, A., Alcalá, C., López, V., 2012. Sediment drifts and cold-water coral reefs in the Patagonian upper and middle continental slope. Mar. Pet. Geol. 36, 70–82. https://doi.org/10.1016/j.marpetgeo.2012.05.008

Naudts, L., Greinert, J., Artemov, Y., Staelens, P., Poort, J., Van Rensbergen, P., De Batist, M., 2006. Geological and morphological setting of 2778 methane seeps in the Dnepr paleo-delta, northwestern Black Sea. Mar. Geol. 227, 177–199. https://doi.org/10.1016/j.margeo.2005.10.005

Nicholson, U., Libby, S., Tappin, D.R., McCarthy, D., 2020. The Subantarctic Front as a sedimentary conveyor belt for tsunamigenic submarine landslides. Mar. Geol. 424, 106161. https://doi.org/10.1016/j.margeo.2020.106161

Ormazabal, J.P., 2022. Estudio sismo-acústico de las cuencas Malvinas y Magallanes offshore y la faja plegada y corrida asociada. Unpublished PhD thesis, University of Buenos Aires.

Ormazabal, J.P., Esteban, F., Principi, S., Bravo, M.E., Palma, F., Isola, J., Bran, D., Tassone, A., 2023. Seabed Faulting Associated with Gas Leakage in the Southern Malvinas Basin and Burdwood Bank, in: First EAGE Conference on South Atlantic Offshore Energy Resources. European Association of Geoscientists & Engineers, pp. 1–6. https://doi.org/10.3997/2214-4609.202381018

Ormazabal, J.P., Isola, J.I., Palma, F.I., Lozano, J.G., Esteban, F.D., Menichetti, M.M., Lodolo, E., Tassone, A.A., 2020. Basement structural control in magallanes-malvinas fold and thrust belt, offshore Argentina. J. South Am. Earth Sci. 103. https://doi.org/10.1016/j.jsames.2020.102708

Ormazabal, J.P., Principi, S., Palma, F.I., Bran, D.M., Isola, J.I., Esteban, F.D., Tassone, A.A., 2024. Neotectonics on the Namuncurá (Burdwood) Bank: Unveiling seafloor strike-slip processes along the North Scotia Ridge. J. Geol. Soc. London. https://doi.org/10.1144/jgs2023-215

Ormazabal, J.P., Tassone, A., Esteban, F., Isola, J., Cayo, L.E., Lozano, J., Menichetti, M., Lodolo, E., 2019. Structure of the wedge-top and foredeep of the Magallanes-Malvinas basins between 62° W and 67° W (SW Atlantic Ocean). J. South Am. Earth Sci. 93, 364–381. https://doi.org/10.1016/j.jsames.2019.04.016

Pape, T., Geprägs, P., Hammerschmidt, S., Wintersteller, P., Wei, J., Fleischmann, T., Bohrmann, G., Kopf, A.J., 2014. Hydrocarbon seepage and its sources at mud volcanoes of the Kumano forearc basin, Nankai Trough subduction zone. Geochemistry, Geophys. Geosystems 15, 2180–2194. https://doi.org/10.1002/2013GC005057

Paull, C.K., Normark, W.R., Ussler, W., Caress, D.W., Keaten, R., 2008. Association among active seafloor deformation, mound formation, and gas hydrate growth and accumulation within the seafloor of the Santa Monica Basin, offshore California. Mar. Geol. 250, 258–275. https://doi.org/10.1016/j.margeo.2008.01.011

Plaza-Faverola, A., Keiding, M., 2019. Correlation between tectonic stress regimes and methane seepage on the western Svalbard margin. Solid Earth 10, 79–94. https://doi.org/10.5194/se-10-79-2019

Plaza-Faverola, A., Pecher, I., Crutchley, G., Barnes, P.M., Bünz, S., Golding, T., Klaeschen, D., Papenberg, C., Bialas, J., 2014. Submarine gas seepage in a mixed contractional and shear deformation regime: Cases from the Hikurangi oblique-subduction margin. Geochemistry, Geophys. Geosystems 15, 416–433. https://doi.org/10.1002/2013GC005082

Raggio, F., Welsink, H., Fiptiani, N., Prayitno, W., Gerster, R., 2011. Cuenca Malvinas. VIII Congr. Explor. y Desarro. Hidrocarburos Simp. Cuencas Argentinas visión actual 1–16.

Reed, D.L., Silver, E.A., Tagudin, J.E., Shipley, T.H., Vrolijk, P., 1990. Relations between mud volcanoes, thrust deformation, slope sedimentation, and gas hydrate, offshore north Panama. Mar. Pet. Geol. 7, 44–54. https://doi.org/10.1016/0264-8172(90)90055-L

Rensbergen, P. Van, Rabaute, A., Colpaert, A., Ghislain, T.S., Mathijs, M., Bruggeman, A., 2007. Fluid migration and fluid seepage in the Connemara field, porcupine basin interpreted from industrial 3D seismic and well data combined with high-resolution site survey data. Int. J. Earth Sci. 96, 185–197. https://doi.org/10.1007/s00531-005-0021-2

Riley, T.R., Carter, A., Leat, P.T., Burton-Johnson, A., Bastias, J., Spikings, R.A., Tate, A.J., Bristow, C.S., 2019. Geochronology and geochemistry of the northern Scotia Sea: A revised interpretation of the North and West Scotia ridge junction. Earth Planet. Sci. Lett. 518, 136–147. https://doi.org/10.1016/j.epsl.2019.04.031

Sahling, H., Bohrmann, G., Artemov, Y.G., Bahr, A., Brüning, M., Klapp, S.A., Klaucke, I., Kozlova, E., Nikolovska, A., Pape, T., Reitz, A., Wallmann, K., 2009. Vodyanitskii mud volcano, Sorokin trough, Black Sea: Geological characterization and quantification of gas bubble streams. Mar. Pet. Geol. 26, 1799–1811.

https://doi.org/10.1016/j.marpetgeo.2009.01.010

Sahling, H., Masson, D.G., Ranero, C.R., Hühnerbach, V., Weinrebe, W., Klaucke, I., Bürk, D., Brückmann, W., Suess, E., 2008. Fluid seepage at the continental margin offshore Costa Rica and southern Nicaragua. Geochemistry, Geophys. Geosystems 9. https://doi.org/10.1029/2008GC001978

Sánchez Guillamón, O., Palomino, D., Vázquez, J.T., León, R., Fernández-Puga, M.C., López-González, N., Medialdea, T., Fernández-Salas, L.M., Somoza, L., 2023. Morpho-sedimentary structure of new mud volcanoes on the Moroccan Atlantic continental margin (Gulf of Cadiz). Mar. Pet. Geol. 148, 106031. https://doi.org/10.1016/j.marpetgeo.2022.106031

Savini, A., Malinverno, E., Etiope, G., Tessarolo, C., Corselli, C., 2009. Shallow seep-related seafloor features along the Malta plateau (Sicily channel - Mediterranean Sea): Morphologies and geo-environmental control of their distribution. Mar. Pet. Geol. 26, 1831–1848. https://doi.org/10.1016/j.marpetgeo.2009.04.003

Serié, C., Huuse, M., Schødt, N.H., 2012. Gas hydrate pingoes: Deep seafloor evidence of focused fluid flow on continental margins. Geology 40, 207–210. https://doi.org/10.1130/G32690.1

Sha, Z., Liang, J., Zhang, G., Yang, S., Lu, J., Zhang, Z., McConnell, D.R., Humphrey, G., 2015. A seepage gas hydrate system in northern South China Sea: Seismic and well log interpretations. Mar. Geol. 366, 69–78. https://doi.org/10.1016/j.margeo.2015.04.006

Shedd, W., Boswell, R., Frye, M., Godfriaux, P., Kramer, K., 2012. Occurrence and nature of " bottom simulating reflectors" in the northern Gulf of Mexico. Mar. Pet. Geol. 34, 31–40. https://doi.org/10.1016/j.marpetgeo.2011.08.005

Shipley, T.H., Houston, M.H., Buffler, R.T., 1979. Widespread occurrence of possible gas-hydrate horizons from continental slopes as identified on seismic reflection profiles. Proc. Annu.

Offshore Technol. Conf. 1979-May, 1879–1886. https://doi.org/10.4043/3570-ms

Somoza, L., León, R., Medialdea, T., Pérez, L.F., González, F.J., Maldonado, A., 2014. Seafloor mounds, craters and depressions linked to seismic chimneys breaching fossilized diagenetic bottom simulating reflectors in the central and southern Scotia Sea, Antarctica. Glob. Planet. Change 123, 359–373. https://doi.org/10.1016/j.gloplacha.2014.08.004

Somoza, L., Medialdea, T., León, R., Ercilla, G., Vázquez, J.T., Farran, M., Hernández-Molina, J., González, J., Juan, C., Fernández-Puga, M.C., 2012. Structure of mud volcano systems and pockmarks in the region of the Ceuta Contourite Depositional System (Western Alborán Sea). Mar. Geol. 332–334, 4–26. https://doi.org/10.1016/j.margeo.2012.06.002

Soto, J.I., Hudec, M.R., 2023. Mud volcanoes guided by thrusting in compressional settings. Geology 51, 779–784. https://doi.org/10.1130/G51235.1

Talukder, A.R., 2012. Review of submarine cold seep plumbing systems: Leakage to seepage and venting. Terra Nov. 24, 255–272. https://doi.org/10.1111/j.1365-3121.2012.01066.x

Tassone, A., Lodolo, E., Menichetti, M., Yagupsky, D., Vilas, J.F., 2008. Seismostratigraphic and structural setting of the Malvinas Basin and its southern margin (Tierra del fuego Atlantic offshore). Geol. Acta 6, 55–67. https://doi.org/10.1344/105.000000241

Tinivella, U., Giustiniani, M., 2012. An Overview of Mud Volcanoes Associated to Gas Hydrate System, in: Updates in Volcanology - New Advances in Understanding Volcanic Systems. InTech, p. 13. https://doi.org/10.5772/51270

Torres Carbonell, P.J., Dimieri, L. V., Olivero, E.B., Bohoyo, F., Galindo-Zaldívar, J., 2014. Structure and tectonic evolution of the Fuegian Andes (southernmost South America) in the framework of the Scotia Arc development. Glob. Planet. Change 123, 174–188. https://doi.org/10.1016/j.gloplacha.2014.07.019

Tóth, Z., Spieß, V., Jensen, J.B., 2014. Seismo-acoustic signatures of shallow free gas in the

Bornholm Basin, Baltic Sea. Cont. Shelf Res. 88, 228–239. https://doi.org/10.1016/j.csr.2014.08.007

Uliana, M.A., Biddle, K.T., Cerdan, J., 1989. Mesozoic Extension and the Formation of Argentine Sedimentary Basins, in: Extensional Tectonics and Stratigraphy of the North Atlantic Margins. American Association of Petroleum Geologists, pp. 599–614. https://doi.org/10.1306/M46497C39

Van Rensbergen, P., Depreiter, D., Pannemans, B., Moerkerke, G., Van Rooij, D., Marsset, B., Akhmanov, G., Blinova, V., Ivanov, M., Rachidi, M., Magalhaes, V., Pinheiro, L., Cunha, M., Henriet, J.P., 2005. The El Arraiche mud volcano field at the Moroccan Atlantic slope, Gulf of Cadiz. Mar. Geol. 219, 1–17. https://doi.org/10.1016/j.margeo.2005.04.007

Volpi, V., Civile, D., Lodolo, E., Romeo, R., Accettella, D., Accaino, F., Ferrante, G.M., 2022. Seabed and shallow morphological setting of the western Sicilian Channel. Bull. Geophys. Oceanogr. 63, 357–376. https://doi.org/10.4430/bgo00401

Wildish, D.J., Akagi, H.M., McKeown, D.L., Pohle, G.W., 2008. Pockmarks influence benthic communities in Passamaquoddy Bay, Bay of Fundy, Canada. Mar. Ecol. Prog. Ser. 357, 51–65. https://doi.org/10.3354/meps07331

Wrather, W.E., Lahee, F.H., 1934. Problems of Petroleum Geology. American Association of Petroleum Geologists. https://doi.org/10.1306/SV6334

Yang, J., Lu, M., Yao, Z., Wang, M., Lu, S., Qi, N., Xia, Y., 2021. A Geophysical Review of the Seabed Methane Seepage Features and Their Relationship with Gas Hydrate Systems. Geofluids 2021, 1–26. https://doi.org/10.1155/2021/9953026

Yrigoyen, M.R., 1989. Cuenca de Malvinas, in: Chebli, G., Spalletti, L. (Eds.), Cuencas Sedimentarias Argentinas. Universidad Nacional de Tucumán, pp. 481–491.

Declaration of interests

☒ The authors declare that they have no known competing financial interests or personal relationships that could have appeared to influence the work reported in this paper.

☐The authors declare the following financial interests/personal relationships which may be considered as potential competing interests: